ACS Catalysis

Review

Cite This: ACS Catal. 2019, 9, 10126−10141

pubs.acs.org/acscatalysis

Recent Insights into the Oxygen-Reduction Electrocatalysis of Fe/N/C Materials

Wang Wang,[†,‡] Qingying Jia,[*,‡] Sanjeev Mukerjee,[*,‡] and Shengli Chen[*,†]

[†]Hubei Electrochemical Power Sources Key Laboratory, Department of Chemistry, Wuhan University, Wuhan 430072, China

[‡]Department of Chemistry and Chemical Biology, Northeastern University Center for Renewable Energy Technology, 317 Egan Research Center, 360 Huntington Avenue, Boston, Massachusetts 02115, United States

ABSTRACT: Owing to the high activity toward the oxygen reduction reaction (ORR) and the selectivity toward the four-electron pathway, single atom Fe/N/C electrocatalysts have been considered as the most promising low-cost candidates to replace Pt in fuel cells. Despite the significant progress achieved in the past decade, the performance and durability of Fe/N/C catalysts remain far behind that of the Pt-based materials in practical devices such as proton exchange membrane fuel cells (PEMFCs) in light-duty vehicles. Recent progress in Fe/N/C electrocatalysis has been mainly based on the empirical approach with rather random combinational synthesis conditions and precursors. For rational design of applicable Fe/N/C catalysts, an insightful understanding of fundamental electrocatalysis of Fe/N/C is required. In this critical review, we will focus on the mechanisms of the ORR catalysis of Fe/N/C, the categories of active sites in Fe/N/C catalysts including the electronic and structural properties of the catalytic centers, the assessment and quantification of the active sites, pH effect on the activity, and the degradation mechanisms. We hope the comprehensive and thorough discussions of Fe/N/C electrocatalysis will help to guide the design and development of high-performance Fe/N/C electrocatalysts toward the application of PEMFCs.

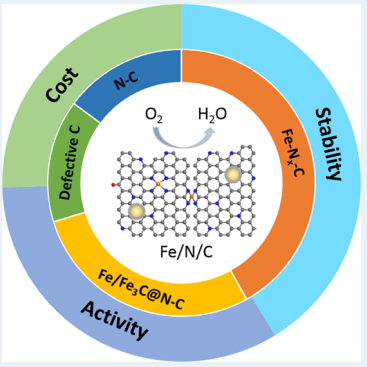

KEYWORDS: *oxygen reduction reaction, Fe/N/C electrocatalysts, catalysis mechanism, active sites, pH effect, stability, fuel cell*

1. INTRODUCTION

With the increasing concerns of global warming and climate change related to the worldwide consumption of fossil fuels, the search for and development of sustainable and clean energy storage and conversion technologies is a key focus of today's world.[1−5] High-capacity energy conversion systems, such as proton exchange membrane fuel cells (PEMFCs), have aroused extensive research interests because of their low or zero emissions and high efficiency.[6−8] The oxygen reduction reaction (ORR) is the key reaction of these advanced energy technologies. However, the sluggish kinetics of this multi-electron transfer process requires a significant amount of electrocatalysis for acceleration. Platinum (Pt) group materials (PGM catalysts) and PGM-free catalysts (mainly the transition metal and N-doped carbon materials) are two frontier groups of efficient electrocatalysts for ORR.[9−12] These two groups have their own advantages and drawbacks, based on which the U.S. Department of Energy (DOE) has proposed specified technical goals and objectives to advance fuel cell technologies for transportation, stationary, and early market applications.[13,14] To compete with the alternative powertrains including the advanced gasoline engines, the DOE planned the fuel cell system targets for light-duty vehicle transportation, including the energy efficiency, power density, start time from low temperature, cost, and durability as shown in Figure 1.[14] To meet these targets, specific requirements for all the components of the fuel cell stack system have been set. From the perspective of the electrocatalysts, the technical targets are

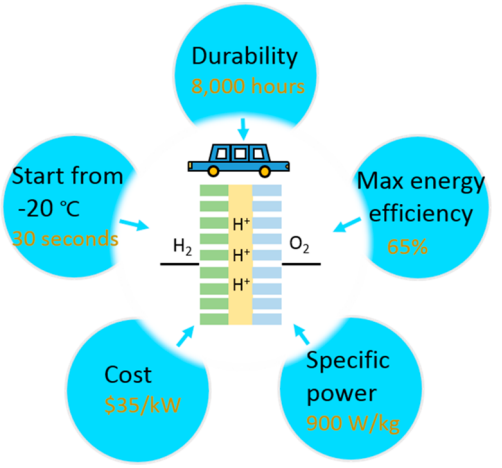

Figure 1. The 2025 targets (yellow) for light-duty vehicle applications. Cost status is for a modeled system when manufactured at a volume of 500 000 units/year.[14]

summarized in Table 1. The 2025 activity target for PGM catalysts is ≤0.10 g/kW@150 kPa for the whole cell, and the mass activity target is 0.44 A/mg PGM@0.9 $V_{iR\text{-free}}$. These targets for PGM-based membrane electrode assembly (MEA)

Received: June 19, 2019
Revised: August 20, 2019
Published: September 26, 2019

DOI: 10.1021/acscatal.9b02583
ACS Catal. 2019, 9, 10126−10141

Table 1. Technical Targets: Electrocatalysts for Transportation Application[a]

characteristic	units	2017 status	2025 target
PGM total content of the whole cell	g/kW @150 kPa	0.125	≤0.1
mass activity	A/mg PGM @900 $mV_{iR\text{-free}}$	0.6	0.44
loss in initial activity	% mass activity loss	40	≤40
loss in performance at 0.8 A/cm^2	mV	20	≤30
electrocatalyst support stability	% mass activity loss	not tested	≤40
loss in performance at 1.5 A/cm^2	mV	>500	≤30
PGM-free catalyst activity	A/cm^2 @0.9 $V_{iR\text{-free}}$	0.021	0.044

[a]Proposed by the DOE in 2017.[14] Test conditions: H_2/O_2, anode stoichiometry 2, cathode stoichiometry 9.5, 150 kPa, 80 °C, fully humidified gases.

have almost been fulfilled according to the data collected in 2017.[15] The major challenges of Pt-based MEAs are the cost and durability. According to a study by the DOE, about 56% of the cost in a fuel cell stack comes from the Pt-based materials because of the scarcity and high price of Pt,[16,17] hindering global commercialization of PGM-based PEMFCs. Another challenging issue for PGM catalysts is the poor durability of Pt under the highly aggressive operating conditions caused by issues such as the Pt dissolution, sintering, and agglomeration of the Pt nanoparticles, which will inevitably lead to the decrease of electrochemical surface area (ECSA) and ORR performance loss.[18,19] Moreover, the Pt is easily deactivated by carbon monoxide (CO) poisoning. Even a trace amount of CO (10−20 ppm) in the fuel can block most of the surface Pt sites.[20,21] At this juncture, tremendous efforts have been devoted to the exploration of advanced and low-cost electrocatalysts with earth-abundant elements. The Fe- and N-doped carbon (Fe/N/C) materials have been regarded as the most promising PGM-free electrocatalysts to substitute Pt because of the comparably high activity and four-electron selectivity toward ORR. The state-of-the-art activity of Fe/N/C electrocatalysts (0.021 A/cm^2@0.9 $V_{iR\text{-free}}$) is far behind the target of 2025 (0.044 A/cm^2@0.9 $V_{iR\text{-free}}$). Moreover, the state-of-the-art durability of the Fe/N/C catalysts in PEMFCs (the performance loss up to 50% in the initial few hours) can hardly meet the durability target of 8000 h drive cycle with startup/shutdown or equivalent accelerated stress test procedures. Therefore, there is large performance improvement space for the Fe/N/C electrocatalysts.

The studies on Fe/N/C catalysts can be traced back to the pioneering work of Jasinski in 1964,[22] which discovered the ORR activity of cobalt phthalocyanine in alkaline conditions, which initiated the research on iron phthalocyanine and iron porphyrin. Following these pioneering works, activity enhancement of $Fe-N_4$ macrocycles adsorbed on carbon was observed after pyrolysis above 700 °C, leading to a new category of catalysts labeled Fe/N/C.[23,24] Later, it was found that such catalysts could be synthesized through the heat treatment of the mixture of individual iron salts, nitrogen sources (aromatic or aliphatic ligands or other N-rich molecules), and carbon precursors with trial-and-error or combinatorial approaches, which led to booming research on Fe/N/C catalysts.[25−27] Through various methods, highly active and moderately stable Fe/N/C catalysts have been successfully developed.[28] However, further development and optimization of the Fe/N/C catalysts are hindered by the lack of the fundamental understanding of the catalytic mechanism and precise chemistry of active sites.[29−32] The simultaneous presence of multiple heterogeneous organic and inorganic moieties, complex electronic and geometric properties of the metal ion, and surrounding environments within the catalysts make it rather difficult to characterize the structure and elucidate the nature of catalytic sites.[33] Therefore, substantial efforts have been devoted to developing various in situ and ex situ techniques, such as X-ray absorption spectroscopy (XAS),[34] time-of-flight secondary ion mass spectroscopy (ToF-SIMS),[35] Mössbauer spectroscopy,[36,37] and X-ray photoelectron spectroscopy (XPS), as well as theoretical calculations,[38] and to designing well-defined structures, like exclusive presence of

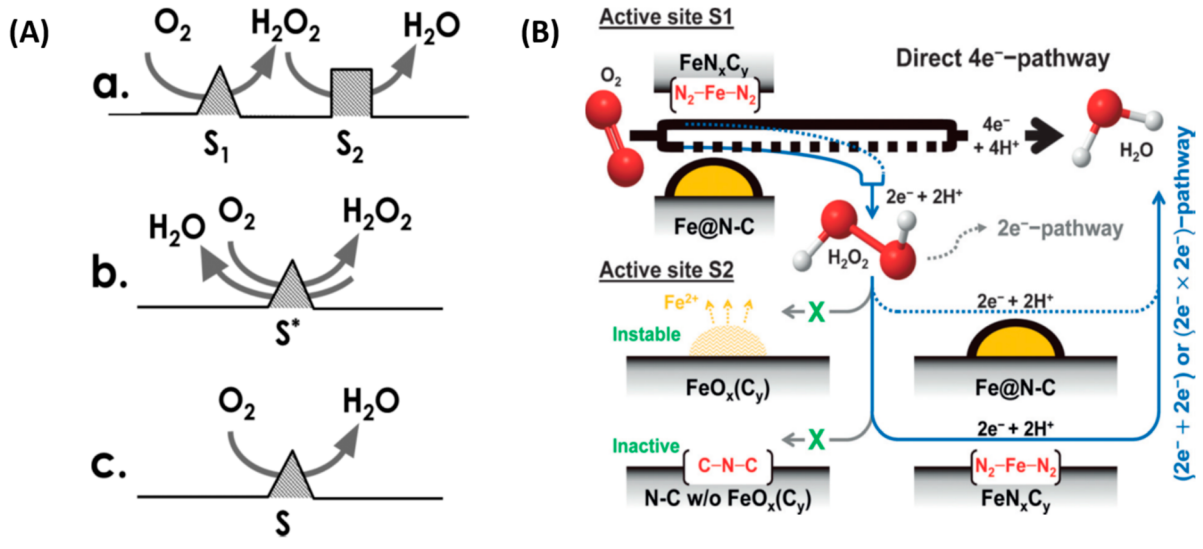

Figure 2. (A) Possible active sites and ORR reaction pathways. (a) Dual-site 2 × 2e⁻. (b) Single site 2e⁻+ 2e⁻. (c) Direct 4e⁻ site. Reproduced from ref 44. Copyright 2015 American Chemical Society. (B) ORR mechanisms on Fe/N/C catalysts in acid medium. Reproduced with permission from ref 45. Copyright 2017 John Wiley & Sons, Inc.

DOI: 10.1021/acscatal.9b02583
ACS Catal. 2019, 9, 10126−10141

FeN_4 sites or model catalysts to do the structural characterization and analysis.[39] Previous reviews mainly focused on the progress in the optimization of synthesis, activity, and catalyst structure; the reaction mechanism and principles of ORR and the nature of catalytic sites have been rarely summarized and reviewed.[27,40,41] For the rational design and optimization of the Fe/N/C catalysts, it is highly desirable to provide timely updates of this field with emphasis on the understanding of active sites in Fe/N/C catalysts, as well as insights into the degradation mechanisms.

In this review, we present the recent progress in the investigation of catalytic sites of M/N/C catalysts (mainly Fe/N/C) in both experimental and theoretical aspects. We aim to categorize and compare the nature of various active sites and the corresponding ORR mechanisms based on the analysis of the breakthroughs achieved so far. This review will cover the ORR catalysis mechanisms, pH effect on the activity, the categories of active sites within the Fe/N/C catalysts including the electronic and geometrical structure of active centers, and the assessment and quantification of active sites, as well as the degradation mechanisms of the Fe/N/C catalysts.

2. ORR MECHANISM HYPOTHESIS

A detailed understanding of the ORR mechanism is highly desirable but challenging owing to the complexity of the ORR process, and the ORR mechanisms depend primarily on the properties of the electrode surfaces.[5,42] Generally, the O_2 molecule can be reduced through the direct $4e^-$ pathway to H_2O (in acid) or OH^- (in alkaline) or the $2e^-$ pathway to H_2O_2 or HO_2^- and an indirect $4e^-$ pathway to H_2O (in acid) or OH^- (in alkaline).[43] Owing to the simultaneous presence of various active sites with different structural motifs, multiple ORR pathways may coexist for the Fe/N/C catalyst surfaces as depicted in Figure 2A.[44] Site 1 (S_1) can reduce O_2 to the H_2O_2 intermediate by the $2e^-$ pathway, and the H_2O_2 could diffuse away or be captured by another site (S_2) and reduced to H_2O through another $2e^-$ step. This process is denoted as the dual-site $2 \times 2e^-$ pathway. An alternative indirect $4e^-$ pathway is the single site $2e^- + 2e^-$ mechanism, where O_2 is reduced to H_2O_2 through a $2e^-$ step and further reduced to H_2O on the same site. The ideal pathway to get high efficiency in power generation would be the direct $4e^-$ reduction pathway without H_2O_2 produced in a $2e^-$ step. Another reason why H_2O_2 intermediate production should be avoided is that the H_2O_2 will also cause instability of the Fe/N/C catalysts during long-term operation, which will be discussed later.

It is challenging to elucidate the ORR pathways occurring on the Fe/N/C because of the coexistence of multiple types of surface chemical moieties (Figure 2B).[45] There is a growing consensus that square-planar $Fe(II)N_4$ sites catalyze the O_2 reduction in acid through a $4e^-$ pathway with a H_2O_2 yield as low as that measured for Pt/C catalysts (1−2%).[46] Tylus et al. argued that the $Fe^{2+}-N_4$ centers catalyze the ORR through a single-site $2e^- + 2e^-$ mechanism in alkaline media and the dual-site $2 \times 2e^-$ mechanism in acid media with a significant role for the surface-bound, coexisting Fe/Fe_xO_y nanoparticles (NPs) as the secondary active site for hydrogen peroxide reduction as shown in Figure 3.[47] On the other hand, Kattel and Wang predicted based on first-principal density functional theory (DFT) calculations that the most kinetically favorable pathway on FeN_4 is the $4e^-$ OOH dissociation pathway, in which the rate-determining step is the OOH dissociation reaction.[48]

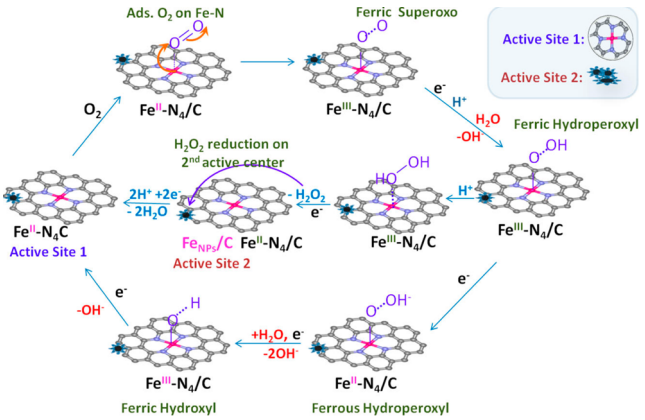

Figure 3. Proposed ORR mechanistic pathways on $Fe-N_4/C$ and adjacent Fe_{NPS}/C in acidic (H^+) and alkaline ($H_2O/-OH$) electrolyte. Reproduced with permission from ref 47. Copyright 2014 American Chemical Society.

For N-doped carbon in acid, the ORR may follow a $2e^- + 2e^-$ pathway or a direct $4e^-$ pathway on the carbon atom next to the N,[49] while the H_2O_2 percentage can be as high as 30%.[50,51] The H_2O_2 yield may decrease dramatically when inorganic species such as Fe/Fe_xC are wrapped by a N-doped carbon overlayer because of the stabilization of the H_2O_2 intermediate by the inorganic moiety sublayer.[52] In contrast, it has been argued that N-doped carbon free of Fe and Fe particles exposed to the electrolyte is inactive toward H_2O_2 reduction in acid;[45] thus a $2e^-$ pathway may be followed. The doping of the heteroatoms such as Fe and N into the graphene plane would lead to the redistribution of the charge and spin density of the carbon plane. The actual adsorption site for the heteroatom-doped carbon depends on the adsorption energy of the oxygen-containing species. For example, the Fe center is believed to be the active site for the $Fe-N_x-C$ coordination structures because the oxygenates are adsorbed more favorably on the Fe site than the N and C sites. In N-doped carbon, the C site adjacent to the N atom is believed to be active site owing to the comparatively optimized adsorption energy.

3. CATEGORIES OF THE CATALYTIC CENTERS

The exact nature of the catalytic centers induced by high-temperature pyrolysis is still a complex and elusive topic. The respective roles of Fe, N, and C elements with different possible combinations in the catalyst toward the catalysis of the ORR have been controversial ever since. For example, the role of iron has been debated for decades.[53,54] Some argued that such high activities of the catalysts with very limited surface content of Fe (<0.1 atom %) can exclude the possibility of Fe being a component of the active site.[55−57] It was proposed that the presence of Fe is responsible for catalyzing the formation of some particular nitrogen functionalities, which are the principal active sites toward ORR.[58,59] However, with the application of small probe molecules or anions such as cyanide, it has been acknowledged that iron plays an indispensable role in the catalysis of ORR.[53,60] The various nitrogen types such as pyridinic, pyrrolic, and graphitic nitrogen,[61] and the different catalyzing behaviors of even the same structural motifs in the Fe/N/C between alkaline and acid conditions have obscured the investigation of the nature of catalytic sites. With the developments of advanced spectroscopic techniques under *in situ* and *ex situ* conditions such as extended X-ray adsorption

DOI: 10.1021/acscatal.9b02583
ACS Catal. 2019, 9, 10126−10141

fine structure (EXAFS) and Fe Mössbauer spectroscopy, the structure−activity relationship has been constructed for different structure motifs and further understanding of the electronic structures as well as the catalyzing mechanisms has been obtained with the help of modeling and DFT calculations. According to the discussion in section 2, we believe that the active sites in Fe/N/C should be the same in different electrolytes across a wide range of pH values. From the perspective of technical maturity of proton exchange membranes, this review will focus on the nature of active sites in acid unless mentioned otherwise.

3.1. Fe−N_x−C Coordination. Extensive research efforts have been devoted to elucidating the role of iron in the Fe/N/C. Although it was under debate whether iron directly participates in the catalysis of ORR, it is now widely accepted that Fe−N_x−C moieties, such as Fe−N_4−C and Fe−N_2−C, are one class of highly active and acid-resistant catalytic centers toward ORR as depicted in Figure 4.[62]

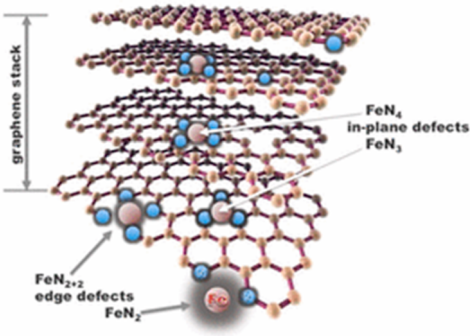

Figure 4. A representation of the graphitic structure with Fe−N_x species is illustrated. Reproduced from ref 62. Copyright 2017 American Chemical Society.

Lefèvre et al. used ToF-SIMS to detect active sites in Fe/N/C catalysts. They revealed that Fe−N_4−C and Fe−N_2−C are simultaneously present in the prepared catalysts. By correlating the ions detected by the ToF-SIMS with the catalytic activity, they found that Fe−N_2−C is more electrocatalytically active than Fe−N_4−C. The abundance of the Fe−N_2−C is dependent on the Fe precursor and pyrolysis temperature.[63] Although no direct experimental proof supports the presence of Fe−N_3−C in Fe/N/C, Kabir et al. proposed that Fe−N_3−C defects are anticipated to be present in the Fe/N/C catalysts at least during pyrolysis based on the DFT calculations and XPS results. The defect abundance according to the formation energies follows the order: Fe−N_4−C > Fe−N_3−C > Fe−N_2−C. They pointed out that Fe−N_3−C geometry is more stable than that of Fe−N_2−C, which was previously observed as a catalytic site for ORR.[64] Despite there being some debate about other Fe−N_x−C structures, the high activity of Fe-N_4-type catalytic sites in Fe/N/C catalysts is undisputable.[65,66] For example, Kramm et al. prepared Fe/N/C catalysts having exclusively Fe−N_4 sites and observed high activity with a high turnover frequency (TOF) of 0.33 e s^{-1} $site^{-1}$ (0.8 V).[39] The carbon-embedded Fe−N_4 structure was directly visualized by aberration-corrected scanning transmission electron microscopy (AB-STEM) and confirmed by the EEL spectra obtained around the Fe atom as illustrated in Figure 5A.[67] Fei et al. also reported the visualization M−N_4 moieties such as Fe−N_4, Co−N_4, and Ni−N_4 as shown in Figure 5B.[68] These results unambiguously proved the existence of the Fe−N_4-type catalytic sites. The development of advanced characterization techniques enabled us to gain deeper insights into the geometry and electronic structure of the Fe−N_4 moiety. For example, van der Kraan et al. shed some light on the geometry and electronic structure by applying *in situ* and *ex situ* Fe Mössbauer spectroscopy on iron tetraphenylporphyrin (FeTPP) heat-treated at different temperatures.[69] Four doublets ascribed to the Fe−N_4 with different iron spin states were observed in all the Fe/N/C catalysts, and it was found that (1) the catalysts prepared under higher temperature are more active than those pyrolyzed under lower temperature, which was attributed to the increased redox potential of iron in the catalysts prepared under higher temperature, and (2) a considerable change of the spectra along with the cyclic voltammetry (CV) with redox peaks ($Fe^{2+/3+}$) probably owing to the variation of the iron oxidation state was observed under different electrode potentials. Based on the respective roles of

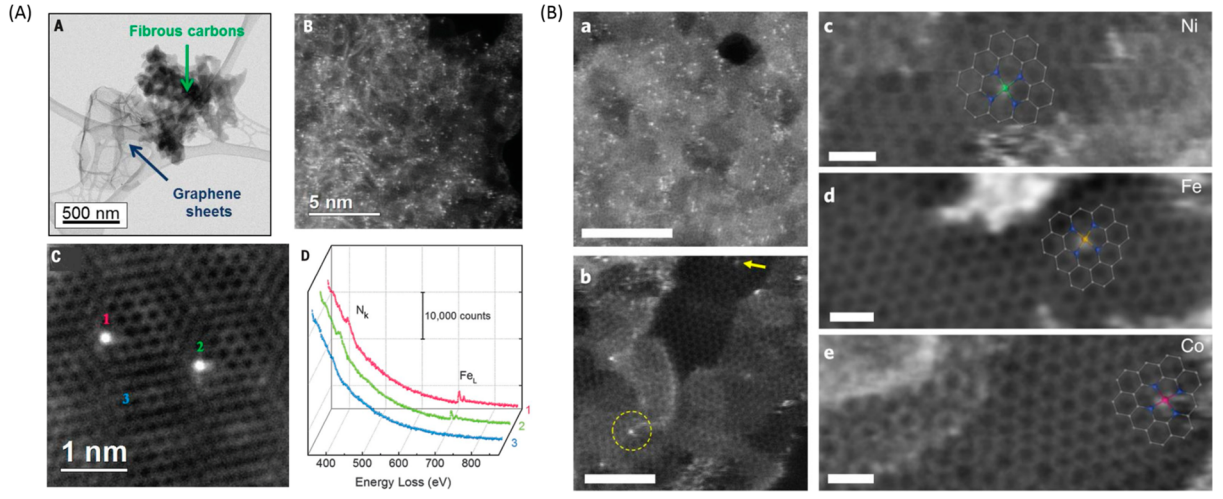

Figure 5. (A) AC-STEM images and EEL spectra of the (CM + PANI)-Fe-C catalyst. From ref 67. Reprinted with permission from AAAS. (B) Atomic structure characterizations of M-NHGFs by annular dark-field STEM. Reprinted by permission from Springer Nature, ref 68, Copyright 2018.

DOI: 10.1021/acscatal.9b02583
ACS Catal. 2019, 9, 10126−10141

Fe, N, and C, several aspects have been investigated about the geometry and electronic structure of the coordination.

3.1.1. The d-Electron Density of the Fe Center. According to the Sabatier principle for catalysis, the highest activity of the catalyst should result from an optimized binding strength between the catalyst and the reaction intermediates, neither too strong nor too weak.[42] The change in the d-electron density of Fe should affect the σ-type bonding between the orbitals of oxygenates ($*O_2$, *OOH, *OH, *O) and the Fe center, thereby influencing the catalytic activity.[70] The change in the 3d-electron density of the iron center (embedded in a specific environment) can be easily detected by the isomer shift in the Fe Mössbauer spectroscopy. Based on the isomer shift of Fe Mössbauer spectroscopy and the binding energy change in X-ray photoelectron spectroscopy, Kramm et al. reported that a partial shift of electron density from the coordinating nitrogen atoms to the iron atom of the Fe−N_4 was caused by the pyrolysis of the FeTMPPCl under higher temperatures, indicating an increase in the 3d-electron density of Fe. Correspondingly, an increase in the TOF of the FeN_4 was observed.[71] Meanwhile, Ramaswamy et al. proposed an opposite origin of the increase of the ORR activity upon pyrolysis.[72] They argued that the pyrolysis of the Fe−N_4 macrocycle (FeTPPCl) would transform the ligand environment from a π-electron-rich macrocycle ring to a π-electron-deficient graphitic ligand, and the electron-withdrawing character causes lower electron density at the Fe center and downshift of the e_g-orbital, leading to higher TOF. This hypothesis was further supported by establishing the relationship between oxygen-reduction turnover number and the Lewis basicity of graphitic carbon support. The electron-withdrawing character of highly disordered graphitic carbon such as ketjen EC600JD can lower the electron density of the metal center, enhancing the TOF of Fe−N_4 from ∼10 s^{-1} $site^{-1}$ to ∼30 s^{-1} $site^{-1}$ in alkaline media. It was believed that the initiation of the ORR process on the Fe−N_4 moiety is mediated by the Fe^{2+}/Fe^{3+} transition: N_4−Fe^{2+} + O_2 ⇔ N_4−Fe^{3+}−O_2^-. The electron-withdrawing property of the carbon support caused an anodic shift in the redox potential of Fe^{2+}/Fe^{3+} and a higher activity. Jiang et al. also reported that the Fe/Fe_3C moieties would interact with the Fe−N_x and reduce the charge density of the central ion, leading to a higher activity.[73] These results suggested that the ORR activity of the Fe−N_x−C coordination can be tuned by the changing the 3d-electron density of the central Fe.

3.1.2. The Geometry of the Fe−N_4. There has been agreement on the paramount importance of nitrogen in the Fe/N/C catalysts within the community, while the type of the nitrogen binding to the Fe center that is most active toward ORR is still under debate. It has been proposed that the pyrolysis of the macrocycle such as iron-porphyrin, in which the nitrogen atoms are pyrrolic, would still retain the Fe−N_4 structure with the concomitant bonding of the pyrrolic part while the ligand is partially destructed as depicted in Figure 6.[69]

Yang et al. also pointed out that the origin of the high activity of the Fe/N/C catalyst is from the Fe−pyrrolic-N_4 species.[74] According to their work, Fe−pyrrolic-N_4 showed higher onset potential (U_{onset}) and exchange current density (j_0) than Pt/C (20 wt %) based on the experimental results in alkaline media. It also exhibited higher U_{onset}, j_0, and $4e^-$ catalysis pathway selectivity than Pt(111) and Fe−pyridinic-N_4 structure. However, these conclusions made by Yang et al.

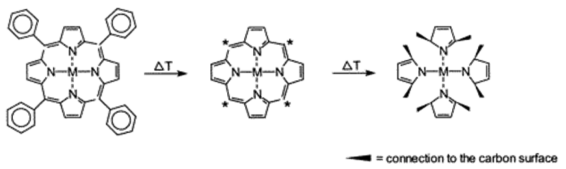

Figure 6. Visualization of the reaction of the porphyrin with the carbon during heat treatment. Reproduced from ref 69. Copyright 2002 American Chemical Society.

were based on the experimental results obtained in alkaline media; the activity of these structures may be quite different in acid media as discussed in section 2. Based on Fe Mössbauer spectroscopy, the Fe−N_4 center with Fe in low-spin state (S = 0) coordinated by four pyrrolic nitrogen atoms (labeled as D1) has been identified by many research groups just as shown in Figure 7A.[75] It has been proposed that the Fe−N_4 is formed in

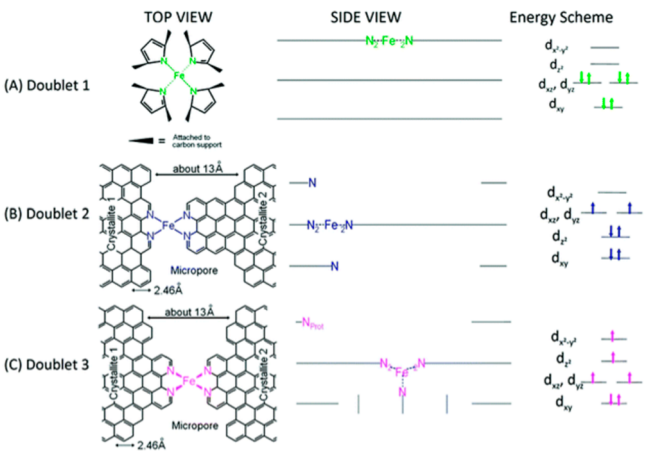

Figure 7. Side views and top views of the proposed structures of (A) the FeN_4/C catalytic site in heat-treated, macrocycle-based catalysts assigned to Mössbauer doublet D1, (B) the FeN_{2+2}-like micropore-hosted site found in the catalyst prepared with iron acetate and heat-treated in ammonia assigned to doublet D2, and (C) the N-FeN_{2+2}-like composite site, where N-FeN_{2+2} is assigned to doublet D3. In all side views, graphene planes are drawn as lines. Reproduced with permission from ref 75. Copyright 2012 Royal Society of Chemistry.

the micropores or slits of carbon with four pyridinic nitrogen functionalities attached to the edges of the graphene. This hypothesis is in accordance with the experience from the synthesis of the Fe/N/C catalysts that the pyridinic N is preferentially formed at the edges of the micropores and slit of the graphene sheet, and sufficient micropores are a requirement in densifying active sites.[28] As shown in Figure 7B,C, the middle spin (S = 1) and high spin (S = 2) Fe−pyridinic-N_4 are suggested in the Fe/N/C catalysts. These structures in the micropores and slits have also been recommended by many research groups experimentally and theoretically.[33,60,76−78] Combining the experimental data (XANES) with the computational fitting, Zitolo et al. revealed the existence of FeN_4C_{12} with a clear arrangement of surrounding carbon atoms. This site is structurally different from the previously proposed Fe−pyridinic-N_4 moieties wherein the pyridinic-N bridges the micropores or slits; the pyrrole-type C_4N ring is expected to be more favorable in bridging the edges of the graphene pores.[46] These structure investigations are based on the stationary analysis of the catalysts without considering the structure changes caused by the oxygenates in the electrolyte

DOI: 10.1021/acscatal.9b02583
ACS Catal. 2019, 9, 10126−10141

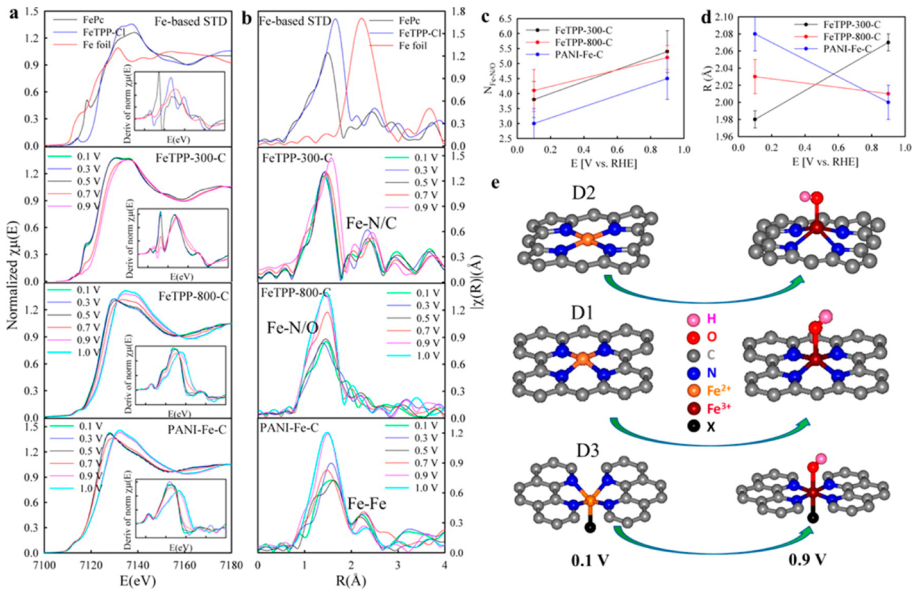

Figure 8. (a) XANES at the Fe K-edge with concomitant first derivatives (insets). (b) The corresponding FT-EXAFS of FeTPP-300-C, FeTPP-800-C, and PANI−Fe−C as a function of applied potentials versus reversible hydrogen electrode. The Fe−N/O coordination numbers (c) and bond distances (d) of FeTPP-300-C, FeTPP-800-C, and PANI−Fe−C at 0.1 and 0.9 V were obtained by EXAFS fits, and the derived Fe−N switching behavior is illustrated by three structural models ($Fe-N_4-C_x$) labeled as D2, D1, and D3, respectively, with/without axially bound $O(H)_{ads}$; the assignment of the doublets might be in different order from that in Figure 7. (e) The atom labeled X represents the fifth ligand with its identity unknown. Reproduced from ref 79. Copyright 2015 American Chemical Society.

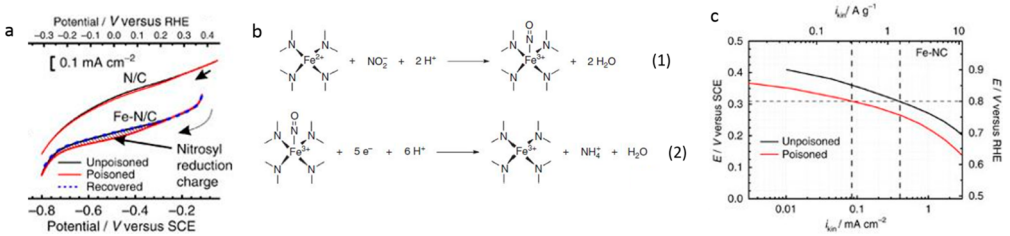

Figure 9. (a) Expansion of the region associated with nitrite stripping. (b) The reactions associated with the nitrite poisoning and reductive stripping. (c) Kinetic current density of Fe/N/C catalyst before and after the poisoning step. Reproduced from ref 88 under terms of Creative Commons license.

and the dynamic potential applied to the catalysts. Jia et al. illustrated the dynamic structure of the $Fe-N_4$ related to the Fe^{2+}/Fe^{3+} redox by recording the bonding distance between different atoms during the catalysis of the ORR process via the *in situ* XANES.[79] As depicted in Figure 8a, the Fe K edge shifts toward higher energy with increasing potential, indicating that all these three catalysts (FeTPP-300-C, FeTPP-800-C and PANI−Fe−C) undergo the Fe^{2+}/Fe^{3+} transition during the ORR catalysis. As summarized in Figure 8b,c,d, the increase of the coordination number and change of the Fe−N/O bond distance are all observed on the three representative catalysts with the increasing potential from 0.1 to 0.9 V. It is interpreted that the $Fe-N_4-C$ center undergoes switching behaviors (Fe moving toward or away from the N_4-plane) during the ORR catalysis. As the most active one among the three catalysts, it is hypothesized that the central Fe is initially out of the N_4-plane in the PANI−Fe−C because of a fifth ligand such as N, which has also been proposed by Kramm et al.[75]

Based on the analysis above,[75] several conclusions were drawn about the ORR on $Fe-N_4-C$ sites:[34,79−82] (1) the ORR rate mediated by the Fe^{2+}/Fe^{3+} redox transition is limited by the removal of oxygen species; the oxygen species is adsorbed upon water activation, $N_x-Fe^{2+} + H_2O \rightarrow N_x-Fe^{3+}-OH_{ad} + e^- + H^+$; thus to make the ORR occur, the adsorbed species must be removed; (2) the catalytical active sites are $Fe^{2+}-N_4$ rather than $Fe^{3+}-N_4$ sites; (3) higher Fe^{2+}/Fe^{3+} redox potential would lead to lower overpotential. Some researchers argued that the oxidation state should be 3+ based on the fact[83] that the Fe/N/C catalysts can be poisoned by SCN^- but not CO because SCN^- can only bind to Fe^{3+} and CO can only bind to Fe^{II} porphyrins. It was pointed out that the CO is not convincing to be used as a probe for Fe/N/C catalysts because unlike the Fe macrocycle, Fe/N/C catalysts are usually resistant to the CO.[84]

3.1.3. The Assessment and Quantification of the Fe−N_x−C Coordination. The turnover frequency (TOF), which is the number of electrons transferred per catalytic site per second, is usually calculated to assess the intrinsic activity of the catalytic site. The single site TOF can be calculated through this equation: TOF (@0.8 V vs RHE) [s^{-1} $site^{-1}$] = $\frac{I_k}{F \times SD}$. I_k (A g^{-1}) is the kinetic current at a certain potential; it can be calculated through the K-L equation: $I_k = \frac{II_L}{I_L - I}$. F (C/mol) is the Faraday constant (96485 C/mol). SD (mol/g) is the density of the electrochemically accessible catalytic sites, which may be obtained from Fe Mössbauer spectroscopy.[85] The

DOI: 10.1021/acscatal.9b02583
ACS Catal. 2019, 9, 10126−10141

average TOF is also calculated to assess the activity:[86] Average TOF (@0.8 V vs RHE) [e^{-1} s^{-1} $site^{-1}$] = $\frac{100MI_k}{ecN}$. M is the molecular weight of Fe, e is the electric charge of a single electron, c is the Fe loading (wt %), and N is Avogadro's number. The calculation of average TOF is based on the metal loading detected by techniques such as X-ray photoelectron spectroscopy (XPS). It is noted that not all the detected metals involved in the catalytic sites are accessible by O_2 and electrolyte. To solve this challenge, Sahraie et al. reported low-temperature CO pulse chemisorption and temperature-programmed desorption to quantify the accessible catalytic sites in the catalysts.[87] Because CO adsorption on metal-free nitrogen functionalities is negligible and the amount of CO adsorbed increases with the ORR activity, it can be deduced that the CO adsorbs predominantly on the metal-containing ORR active sites. Based on this deduction, the TOF_{CO} of the surface accessible catalytic sites was presented as TOF_{CO} (@ 0.8 V) = $I_kF^{-1}N_{CO}{}^{-1}$. N_{CO} is the CO uptake (nmol $mg_{catalyst}{}^{-1}$) of the catalyst. All the adsorption processes were carried out at 193 ± 5 K. Recently, Malko et al. proposed an easy in situ electrochemical method to quantify active sites through nitrite adsorption followed by reductive stripping.[88] As depicted in Figure 9a, an apparent difference was observed for the electrode voltammograms of the NO_2^- poisoned and unpoisoned Fe/N/C catalysts. This difference in current was believed to be caused by the reduction of the adsorbed nitrosyl ligand as shown in Figure 9b. Based on the integrated charge transferred for the nitrosyl stripping, the surface nitrite sensitive site density can be calculated using the following equation: SD (mol g^{-1}) = $\frac{Q(C\ g^{-1})}{nF(C\ mol^{-1})}$. Q is the charge associated with the nitrosyl reduction, and n is the number of electrons transferred for the reduction of one adsorbed nitrosyl per site. Further the TOF of the nitrite sensitive sites can be acquired: TOF (@0.8 V vs RHE) [s^{-1} $site^{-1}$] = $\frac{\Delta I_k}{F \times SD}$. ΔI_k is the kinetic current difference between the nitrite poisoned and unpoisoned electrode as shown in Figure 9c.

As revealed by these methods for the quantification of active sites in Fe/N/C catalysts, the utilization of iron compared to the iron loading is very low (~4.5%). It has been summarized that the activity of the Fe (Co)/N/C catalysts increases with increased metal loading in the range of 0.3−3 wt % because of the saturation of doped nitrogen:[89,90] the number of nitrogen-doped defects that can host metal atom forming active sites is very limited. Therefore, the assessment and quantification of nitrogen as well as the nitrogen content should be given more attention to increase the active site density of M/N/C catalysts.

3.2. N−C_x. The indispensable role of nitrogen (N) in the Fe/N/C materials for the catalysis of ORR has been demonstrated by the researchers.[91] In addition to the formation of Fe−N_x-type catalytic centers, N can be *in situ* doped into the carbon matrix during the pyrolysis. Nitrogen, next to the carbon in the Periodic Table, has a larger electronegativity than carbon (3.04 for N, 2.55 for C).[40] As such, the introduction of N into the carbon sheet can make the neighboring carbon atoms electron deficient and decrease the gap between the Fermi level and conduction band, leading to a higher charge mobility of the graphene lattice. According to the DFT calculations, the intrinsic catalytic activity and ORR mechanism of the heteroatom-doped graphene depends on the charge, spin density and coordinate state of the carbon sites. The spin density effect and charge effect are particularly important in modulating the catalytic activity of the inner carbon sites.[92,93] The redistribution of the charge density and spin density of carbon atoms owing to the N doping has significant effects on oxygenate adsorption and the first electron transfer of ORR.[94,95] It has been well-known that N can mainly form three different configurations when doped into graphene possibly associated with the ORR catalysis, graphitic N, pyridinic N, and pyrrolic N. As depicted in Figure 10, the N directly substitutes the carbon atom and is

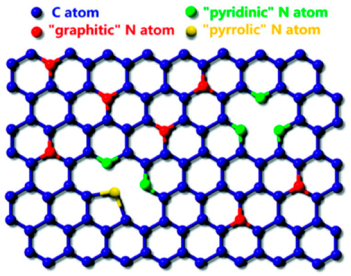

Figure 10. Schematic representation of the N-doped graphene. The blue, red, green, and yellow spheres represent the C, "graphitic" N, "pyridinic" N, and "pyrrolic" N atoms in the N-doped graphene, respectively. Reproduced from ref 96. Copyright 2009 American Chemical Society.

incorporated into a hexagonal ring forming graphitic N and pyridinic N (at the edge), while pyrrolic N (at the edge) is included in a five-membered ring.[96] Graphitic N and pyridinic N are sp^2 hybridized, and pyrrolic is sp^3 hybridized. The debate on the actual active sites regarding the type of N functionalities mainly focuses on the graphitic N and pyridinic N.[50,51,97−99] The conclusions about the active sites have usually been made based on the correlation between the ratio of a certain type of N and the ORR activity through XPS peak fitting. However, the conclusions by such methods can be misguiding if it is not very carefully treated because of the experimental uncertainties and the inhomogeneities associated with the morphology and graphitization level. Recently, Guo et al. recognized the individual contribution from the different types of N by developing highly oriented pyrolytic graphite (HOPG) model catalysts and concluded that the ORR active site in acid is created by the pyridinic N.[49] As shown in Figure 11A−E, ordered edge-patterned HOPGs including pyri-HOPG, grap-HOPG, edge-HOPG, and clean-HOPG were selectively prepared to study the N dopant without influence of morphology. The pyridinic-N-dominated HOPG showed much higher activity than the graphitic-N-dominated HOPG, edge-HOPG, and clean-HOPG. Additionally, the acidic CO_2 was found to adsorb only on the pyri-HOPG, indicating that the Lewis base site is created by the pyridinic N and the carbon atom neighboring the pyridinic N is the active site.

The possible ORR mechanism was also proposed on N-doped carbon (Figure 11G). The adsorption site for O_2 is the carbon atom adjacent to the pyridinic N, and the subsequent ORR can occur through the indirect $4e^-$ process or direct $4e^-$ process. This proposal was partially evidenced by the detected OH species in the post-ORR XPS measurement. Also, Xing et al. reported the observation of OH_{ad} remaining on the carbon atoms neighboring the pyridinic N after ORR measurement and pointed out that the carbon atoms next to the pyridinic N should be the main active sites among other N config-

DOI: 10.1021/acscatal.9b02583
ACS Catal. 2019, 9, 10126−10141

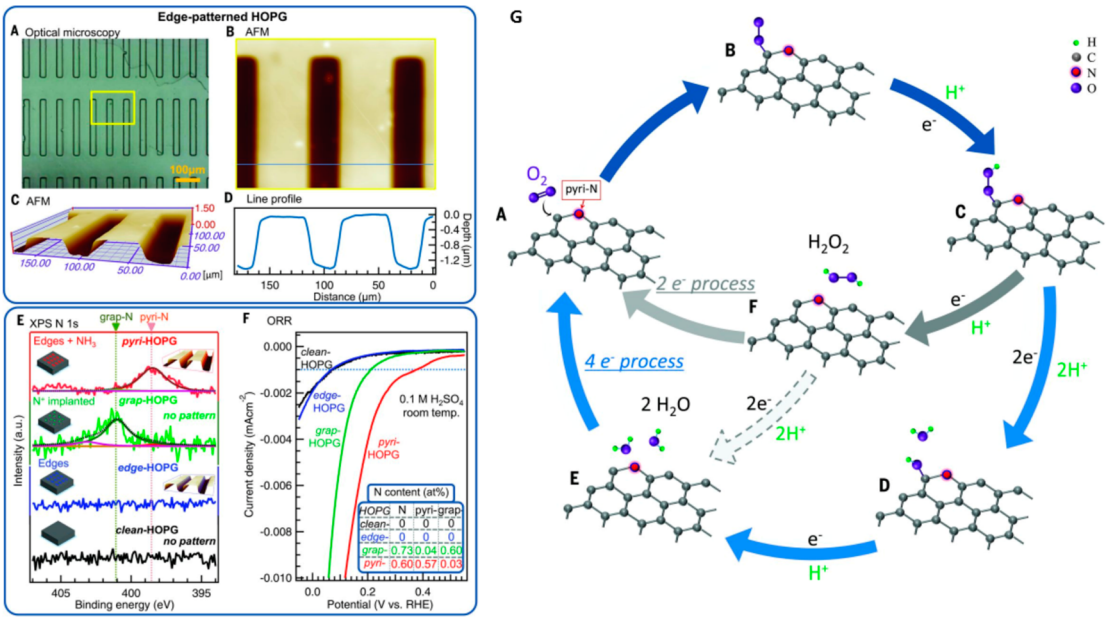

Figure 11. (A) Optical image of patterned edge-N^+−HOPG. (B) The AFM image obtained for the region indicated by the yellow rectangle in panel A. (C) Three-dimensional representation of the image in panel B. (D) Line profile of the AFM image obtained along the blue line in panel B. (E) N 1s XPS spectra of model catalysts. (F) ORR results for model catalysts corresponding to panel E. Nitrogen contents of the model catalysts are shown as the inset in panel F. (G) The schematic pathway for oxygen reduction reaction on nitrogen-doped carbon materials. From ref 49. Reprinted with permission from AAAS.

urations.[100] Among these debates, Kim et al. asserted that the outermost graphitic N among others yields the lowest barrier for the rate-limiting first electron transfer and the highest selectivity toward the four-electron reduction pathway based on the DFT calculations.[101] It was proposed that an interconversion may occur between the pyridinic N and graphitic N during the ORR. Although N-doped carbon is proposed as an active species toward ORR, the activity of N−C is poor in acidic electrolyte with the average potential (vs RHE) of ∼0.7 V at −1 mA cm^{-2} tested on RDEs.[54]

It has been reported by many research groups that the metallic Fe or iron carbide encased in the graphitic layer or N-doped carbon are highly ORR active in both acid and alkaline media,[102−104] for example, Hu et al. reported that Fe_3C encapsulated in the graphitic layer (Figure 12a) exhibited high activity toward ORR with a half wave potential of 0.73 and 0.83 V (vs RHE) in 0.1 M $HClO_4$ and 0.1 M NaOH, respectively.[105] Strickland et al. also found that the core−shell structure of the Fe/Fe_xC inorganic nanoparticles wrapped by the carbon shell manifested high ORR activity. The Fe Mössbauer spectroscopy and in situ XANES revealed that no direct Fe−N coordination was observed and Fe^{2+}/Fe^{3+} transition was not detected (Figure 12b,c),[52] indicating the absence or extremely low content of electroactive Fe−N_x species on the surface.

The DFT calculations (Figure 12d) showed that the catalytic activity of such core−shell structure arises from the increased electron density on the carbon layer leading to a decreased work function on the carbon surface and the introduction of N into the carbon layer can further increase the DOS near the Fermi level and lower the work function.[106] Interestingly, the carbon confined Fe/Fe_xC core−shell structure exhibited impressive stability in the PEMFC; for example, almost no significant performance loss was observed after 10 000 potential cycles.[52,105] This outstanding durability is much better than that of the Fe−N_x−C catalysts, which will be discussed in section 5.

4. THE pH EFFECT

The pH-dependent ORR activity effect is observed on both Fe/N/C and Pt/C catalysts. To elucidate the pH effect on Fe/N/C, we would like to start with the Pt/C catalysts. The ORR activity of Pt/C shows apparent pH dependence,[107] where higher exchange current density and kinetic current density at 0.9 V, smaller Tafel slope, and lower H_2O_2 yield are observed at pH = 1 than pH = 13 (Figure 13A).[108] The understanding of the mechanism of the ORR performance gap between acid and alkaline media is of paramount importance because of its role in the energy conversion technologies. Ramaswamy and Mukerjee explained the activity gap on Pt/C from the perspective of the changes in the electric double layer structure at the electrode/electrolyte interface and electrochemical reaction mechanisms in transitioning from acid to alkaline.[108,109] As depicted in Figure 13B (left), it is argued that the chemisorbed O_2 molecule is reduced at the inner Helmholtz plane (IHP) concerted with the transfer of protons from the outer Helmholtz plane (OHP) to the IHP (Figure 13B-a, left) via an inner-sphere electron transfer (ISET) mechanism in the acid environment, while in the alkaline environment, the O_2 can be reduced via both ISET (Figure 13B-a, right) and outer-sphere electron transfer (OSET) with water as the proton source. For OSET (Figure 13B-b, right), H_2O_2 is produced with specifically adsorbed OH as the bridge for electron transfer. The slower kinetics and higher H_2O_2 yield in alkaline media is attributed to the existence of OSET. Interestingly, Fe/N/C catalysts exhibit opposite pH dependence from the Pt/C. The apparent ORR activity of Fe/N/C catalysts is significantly higher in pH = 13 than in pH = 1 and the H_2O_2 yield is lower at high pH.[109−111] Ramaswamy et al. reported 3−4 orders of magnitude higher ORR activity on Fe/

DOI: 10.1021/acscatal.9b02583
ACS Catal. 2019, 9, 10126−10141

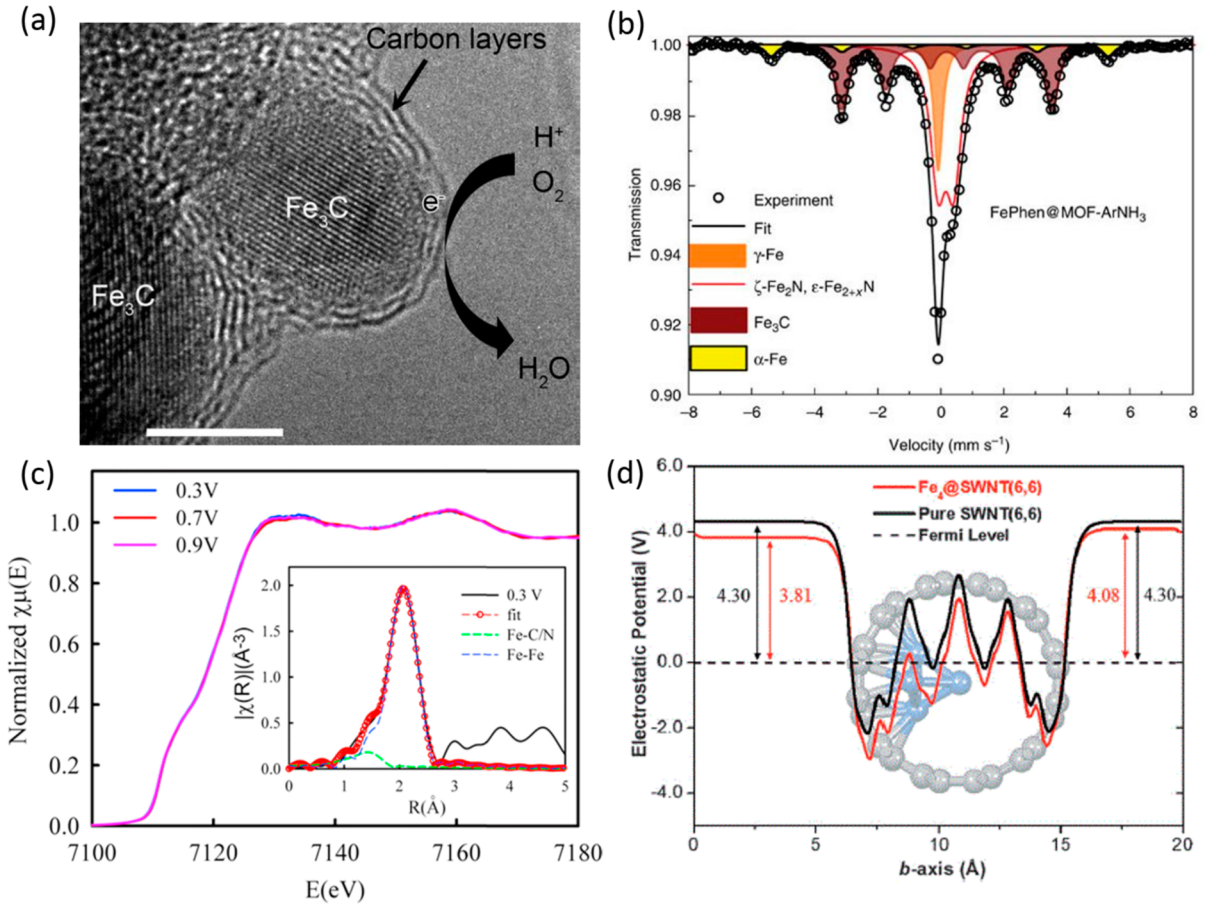

Figure 12. (a) Oxygen reduction process on Fe_3C/C-700 (scale bar = 5.00 nm). Reproduced from ref 105. Copyright 2014 John Wiley & Sons, Inc. (b) Mössbauer absorption spectrum and its deconvolution for the FePhen@MOF-ArNH_3 catalysts. (c) XANES and FT-EXAFS of the Fe K-edge XAS data with the EXAFS fits. Panels b and c reproduced from ref 52 under terms of Creative Commons license. (d) Electrostatic potential profiles averaged on the plane perpendicular to the *b*-axis as a function of the *b*-axis of the supercell of Fe_4@SWNT and pure SWNT, respectively. The structure of Fe_4@SWNT is shown in the background. Reproduced from ref 106. Copyright 2013 John Wiley & Sons, Inc.

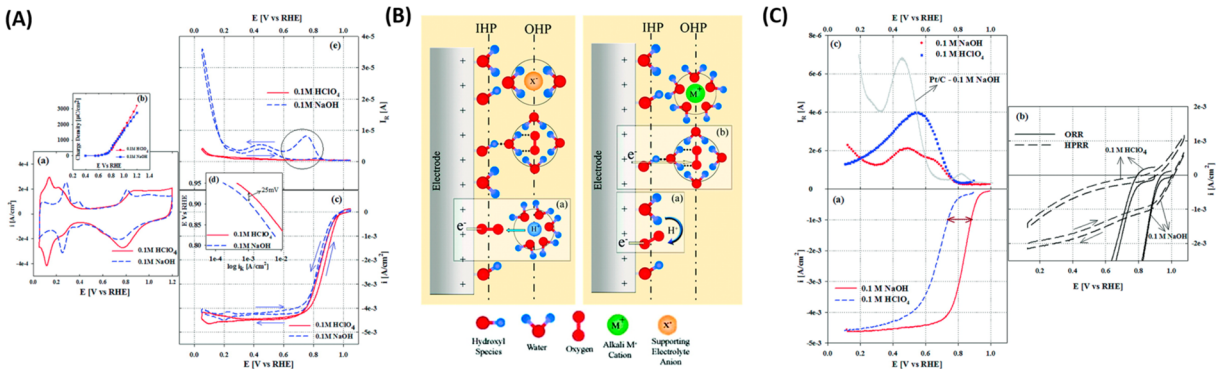

Figure 13. (A) Electrochemical measurements of Pt/C in 0.1 M $HClO_4$ and 0.1 M KOH: (a) cyclic voltammetry in deoxygenated electrolytes; (b) charge density due to oxide formation on Pt; (c) ORR polarization curves at 900 rpm in O_2 saturated electrolytes; (d) mass transport corrected Tafel plots; (e) ring current measured during ORR at 900 rpm. (B) Schematic illustration of the double-layer structure during ORR in acidic (left) and alkaline (right) conditions. Insets a and b illustrate the inner- and outer-sphere electron transfer processes. (C) ORR activity of FeTPP/C catalyst (pyrolyzed at 800 °C) in O_2 saturated acidic and alkaline electrolytes: (a) ORR polarization curves; (b) hydrogen peroxide reduction reaction in comparison to ORR; (c) ring current. Also shown in part c is the ring current profile of 30% Pt/C in 0.1 M NaOH for comparison. Reproduced from ref 108. Copyright 2011 American Chemical Society.

N/C in alkaline than that in acid media (i.e., $E_{1/2}$ = 837 ± 8 mV in 0.1 M NaOH against $E_{1/2}$ = 667 ± 12 mV in 0.1 M $HClO_4$).[72] Meng et al. also found that the activity of their Fe/N/C catalyst is 7−10 times higher at pH = 13 than pH = 1.[107] There are mainly two hypothesis explaining this activity gap. One hypothesis proposes that ISET is promoted and OSET is inhibited on Fe/N/C catalysts in alkaline media. The specifically adsorbed OH_{ad} plays different roles on Pt/C and Fe/N/C. For Pt/C, the OH_{ad} is the bridge for OSET as well as a site blocker for ISET. On the other hand, for Fe/N/C, the

DOI: 10.1021/acscatal.9b02583
ACS Catal. 2019, 9, 10126−10141

OH_{ad} on the Fe^{2+} site acts as a labile ligand that can be easily displaced by molecular O_2. Thus, OSET is inhibited on Fe/N/C in alkaline media, ensuring successful $4e^-$ reduction of O_2 through the ISET mechanism. This difference of the OH_{ad} behavior on Pt/C and Fe/N/C explains the electrochemical phenomenon well: the loop behavior of the polarization curve is not observed on Fe/N/C, while it is very typical for Pt/C.[112] It was further found that the HO_2^- intermediate in alkaline media will be reduced immediately to the $4e^-$ product (Figure 13C-b) owing to the higher stability of the intermediate on the active site in alkaline than in acid media. In acid media, the reduction of H_2O_2 is not kinetically favored because of weak binding of H_2O_2 on the active site, leading to a higher H_2O_2 yield as depicted in Figure 13C.

Another hypothesis is that the protonation of the doped nitrogen atoms hinders the charge delocalization and degrades the ORR activity in acid media.[113] The mean pK_a value measured from the Boehm titration is 6.5 for the prepared Fe/N/C catalyst, which indicates the possibility of a fast protonation of the catalyst in acid especially for the pyridinic N because of a low pK_a of 5.2 for pyridine.[114] Rauf et al. pointed out that the protonation of the pyridinic N can reduce the basicity of the adjacent carbon, thus reducing the O_2 affinity. For $Fe-N_x$, the protonation of nitrogen can also lower the electron density of the Fe center, which may shift the potential of $Fe^{2+/3+}$ redox negatively, resulting a lower ORR activity.[115] Herranz et al. attributed the activity decay of the $Fe-N_4$ in acid medium to the protonation of the nitrogen and the subsequent anion binding (Figure 14A). It is believed that

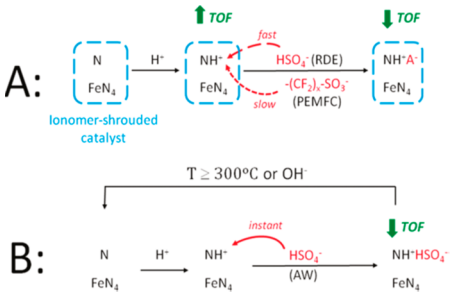

Figure 14. Change of the chemical state of protonable N-groups and simultaneous change of the turnover frequency (TOF) for the ORR of FeN_4 catalytic sites when the Fe/N/C catalyst is shrouded by proton-conducting ionomer (A) or directly in contact with an aqueous acidic solution (B). In case B, the acid-washed catalyst can be reactivated either thermally or chemically. Reproduced from ref 114. Copyright 2011 American Chemical Society.

protonation of the N surrounding the $Fe-N_4$ alone without anion binding will not harm the activity of the $Fe-N_4$, which explains why the initial activity of Fe/N/C in PEMFC (20 A g^{-1}) is much better than that in RDE (3 A g^{-1}). Another observation is that the activity of Fe/N/C catalyst will normally experience 1 order of magnitude decay after acid washing (AW), while the activity can be restored by base washing or thermal treatment with removal of the anion (Figure 14B). From the perspective of the catalytic activity, the $Fe-N_x-C$ coordination structures, Fe/Fe_3C@N−C, N-doped carbon, and defective carbon, are all highly active toward the ORR in the alkaline electrolyte with high half-wave potential of ≥0.8 V (vs RHE) at 3 mA cm^{-2} on RDE. In acid electrolyte, the apparent activity of N-doped carbon and defective carbon materials without iron are nearly negligible. The $Fe-N_x-C$ structures (potential at 3 mA cm^{-2} on RDE ~0.85 V[116]) are much more active than Fe/Fe_3C@N−C (potential at 3 mA cm^{-2} on RDE ~0.78 V[52]). Further understanding and insights into the mechanism of the pH dependence of the Fe/N/C catalysts should be based on the study of the categories of different catalytic sites owing to the heterogeneity of the catalysts synthesized with the traditional pyrolysis method.

5. STABILITY OF THE CATALYSTS IN THE PEMFC

Apart from the modest activity of Fe/N/C catalysts compared to Pt-based materials, the poor durability (especially in the initial few hours, the performance loss can be up to 50%) is another challenging obstacle for the application of PEMFCs.[83,117−120] Almost no N-doped carbon and defective carbon materials are applied to the cathode of the PEMFCs because of the limited activity in acid. The stability is the main issue of the $Fe-N_x-C$ or Fe/Fe_3C@N−C structures. The performance loss has been summarized in this review, and three possible mechanisms will be discussed:

5.1. Carbon Corrosion during the Startup and Shutdown of the Fuel Cell. During the startup and shutdown of the H_2-O_2 fuel cell, an air/H_2 boundary (represented by the dotted line in Figure 15) is formed in the flow channel before H_2 completely fills the channel (e.g., during startup), which drives the oxygen evolution reaction (OER) and carbon oxidation reaction (COR) through the onset of ORR at the anode as depicted in region D.[121,122] The potential of region D will be close to the sum of the potentials of regions B and C, which can reach up to 2 V. Under such high potential, drastic carbon corrosion happens.[123]

This model was originally proposed for Pt materials applied as the cathode catalysts of PEMFCs.[124−127] It is reasonable to believe that the carbon corrosion of the Fe/N/C catalysts may induce even more severe problems leading to performance loss. Unlike the Pt/C catalysts, wherein carbon acts as the conductive support, the carbon matrix in Fe/N/C materials not only serves as the electronic conductor but also hosts the

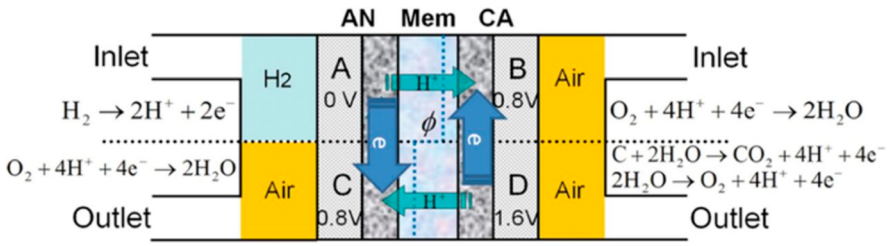

Figure 15. Schematic showing the carbon corrosion scenario during startup/shutdown of a fuel cell. Reproduced with permission from ref 122. Copyright 2015 Electrochemical Society.

DOI: 10.1021/acscatal.9b02583
ACS Catal. 2019, 9, 10126−10141

active species. Consequently, carbon corrosion can induce[128] (1) the loss of the porosity of carbon through the collapse of the catalyst microstructure, which may destroy the active site structure, reducing active site density and even blocking the gas-diffusion pathway toward catalytic center and water removal from the electrode, and (2) the decrease of the hydrophobicity of the catalyst layer. Carbon oxidation may introduce some hydrophilic oxygen groups onto the carbon surface,[129] making the flooding problems even more severe. Recently, Choi et al. studied the Fe/N/C activity degradation mechanism with online inductively coupled plasma mass spectrometry (ICP-MS) and differential electrochemical mass spectroscopy (DEMS) coupled to a modified scanning flow cell (SFC) system.[130] The carbon oxidation of Fe/N/C to CO_2 and CO was observed at high potentials (>0.9 V), which directly caused the destruction of the carbon surfaces and indirectly led to the destruction of active sites. During the operation window of 0.7−0.9 V, the catalysts are stable.

5.2. Attack on Active Sites by H_2O_2. As has been discussed in section 2, the indirect $4e^-$ pathway or $2e^-$ pathway of ORR can generate H_2O_2, which is believed to cause catalyst degradation via the Fenton reaction.[131] Lefèvre and Dodelet immersed a series of catalysts into H_2O_2 solution at various concentrations to mimic the H_2O_2 released in the neighborhood of the catalysts. They observed a dramatic decrease of the activity measured by RDE.[132] For the degradation mechanism, they proposed that radical oxygen species (ROS) destroyed the integrity of the active sites. ROS are strong oxidants and can be formed via the Fenton reaction between H_2O_2 and the transition metal:[133,134] $Fe^{2+} + H_2O_2 \rightarrow Fe^{3+} + HO^{\bullet} + OH^-$; $Fe^{3+} + H_2O_2 \rightarrow Fe^{2+} + HOO^{\bullet} + H^+$. These ROS are believed to be detrimental to the active sites. Goellner et al. reported that the TOF of Fe/N/C decreased more severely than that of Co/N/C after H_2O_2 chemical treatment and that Co/N/C produced less ROS than Fe/N/C when contacted with H_2O_2.[135] Based on the analysis of the change of isomer shift and half-width observed in the Fe Mössbauer spectroscopy after the activity degradation by H_2O_2 contact, Schulenburg et al. proposed that the oxidation and subsequent removal of the coordinating N atoms could cause the loss of the activity.[136] The proposal of activity decay caused by the Fenton-type reaction was further supported by some recent reports: (1) Zelenay and co-workers showed that the simultaneous utilization of Fe and Co precursors in the synthesis of M/N/C catalysts can improve the stability in acid.[137] (2) Carbon or N-doped carbon wrapped Fe/Fe_3C core−shell structure manifested great stability in acid.[52] However, Jaouen et al. found that the exposure of the materials to H_2O_2 leaves the $Fe-N_x-C$ structures intact but decreases their TOF through oxidation of the carbon surface, leading to weakened O_2 binding on iron-based sites.[138] Apart from the adverse effect of H_2O_2 on active sites, it is also proposed that Fenton reactions might cause local ionomer degradation hindering the H^+ transport, which causes the PEMFC performance loss.[139] Altogether, it is agreed that less ROS produced during ORR should enhance the stability of the $Fe-N_x-C$ structures.

5.3. Water Flooding into the Micropores. Dodelet et al. summarized the stability of the PEMFCs based on a series of Fe/N/C electrocatalysts with different microporous surface area/total BET surface area ratio as depicted in Figure 16.[140] The higher fraction of the microporous surface area to the total BET surface area would lead to a faster decay of the cell performance. It was hypothesized that the flooding of the micropores would impede the transport of the oxygen to the active sites hosted in the micropores and cause fast performance loss. This is further supported by their following work.[141] They reported that the durability of the catalysts can be improved by increasing the first pyrolysis temperature from 1050 to 1150 °C. It was explained that increasing the pyrolysis temperature can reduce the hydrophilic character of the carbon matrix and decrease the possibility of water flooding the active sites. Recently, Dodelet's group updated this degradation mechanism of water flooding.[142] They put forward that the flux of water (with dissolved H^+ and O_2) through the open-end micropores caused the demetalation of the $Fe-N_4-C$ sites, which led to the performance loss. It was said that the $Fe-N_4-C$ structure should be quite stable in stagnant acidic media at 80 °C owing to a very small equilibrium constant of the $Fe-N_4-C$ demetalation reaction ($Fe^{2+}-N_4-C_x$,s + $2H^+$,aq ↔ Fe^{2+},aq + $H_2-N_4-C_x$,s); however, the equilibrium will break if the water or humid gas keeps running through micropore channel and takes away the Fe^{2+} according to the Le Chatelier principle. Thus, the structure of the active sites would be destroyed.

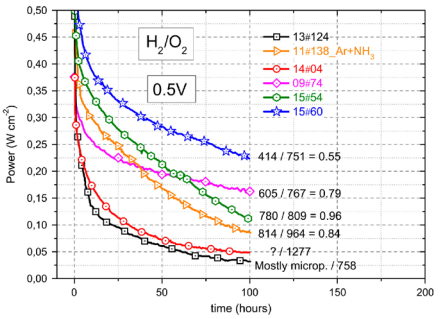

Figure 16. Time evolution in H_2/O_2 fuel cell of the power developed at 0.5 V by several catalysts. The numbers appearing at the end of each curve are the microporous surface area/total BET surface area of each catalyst and their ratio.[140] Reprinted from ref 140, Copyright 2016, with permission from Elsevier.

It is likely that the degradation of most Fe/N/C catalysts in PEMFCs is caused not one mechanism but rather by the combination of the mechanisms mentioned above or undiscovered. In addition, these degradation pathways may have influence on each other. For example, the occurrence of carbon oxidation may promote other degradation pathways; for example, carbon oxidation can decrease the hydrophobicity of the catalyst surface, which further exacerbates the water flooding of the micropores.

6. SUMMARY AND CONCLUSIONS

In this review, a summary of the recent insights into electrocatalysis on Fe/N/C catalysts is provided. The active sites can be mainly classified into two groups: $Fe-N_x-C$ (x = 2, 3, 4) and N−C. For the $Fe-N_x-C$ sites, $Fe-N_4$ hosted in the micropores within the graphene plane or between the slits of two graphene sheets are considered as the predominant active sites with high TOF as well as four-electron-transfer selectivity. The ORR on $Fe-N_4-C$ is initiated by the Fe^{2+}/Fe^{3+} redox transition, accompanied by switching behavior of Fe moving away from or toward the N_4-C plane. Therefore, it is promising to further improve the activity of $Fe-N_4$ by tuning the electronic and geometric structure to shift the Fe^{2+}/Fe^{3+} redox transition positively.

DOI: 10.1021/acscatal.9b02583
ACS Catal. 2019, 9, 10126−10141

For the N−C group catalytic sites, the carbon atom with Lewis basicity adjacent to pyridinic N is regarded as the catalytic center in acid. However, poor activity and low $4e^-$ selectivity of ORR is observed on N−C with a high yield of H_2O_2 in acid medium. The wrapping of the Fe or Fe_3C nanoparticles into the N−C shell forming a core−shell structure without direct exposure of Fe to the electrolyte can boost the activity of N−C owing to the increased DOS near the Fermi level and lowered work function. Also, the stability of Fe/Fe_3C@N−C seems to be better.

The pH effect on the activity of Fe/N/C catalysts (much better activity of Fe/N/C catalysts in alkaline than in acid media) can be mainly attributed to two reasons: (1) ISET is promoted and OSET is inhibited on Fe/N/C in acid electrolyte. (2) Protonation of the N in acid electrolyte hinders the charge delocalization of the active sites and leads to activity loss. For the assessment of the intrinsic activity (calculation of TOF), the accessible active site density can be quantified through the interaction between the Fe center and adsorbates such as nitrite or low-temperature CO, but this method is limited to the active sites with Fe centers. In acid medium, the apparent activity of N-doped carbon and defective carbon materials without iron is almost negligible. The $Fe-N_x-C$ structures (potential at 3 mA cm^{-2} on RDE ~0.85 V) are much more active than Fe/Fe_3C@N−C (potential at 3 mA cm^{-2} on RDE ~0.78 V).

Apart from the activity issues, the poor stability of Fe/N/C in PEMFCs is another problem impeding the commercialization of Fe/N/C materials. The degradation could be caused by oxidation of the carbon matrix or destruction of the active sites via the Fenton reaction, as well as micropore flooding. Thus, to improve the durability, the production of the H_2O_2 intermediate should be avoided and carbon oxidation should be alleviated. For the advancement of plausible Fe/N/C electrocatalysts, more efforts could be devoted to (1) increasing the mass activity by increasing the TOF of active sites or increasing the active sites density; tuning of the d-electron density and geometry of the Fe center and designing of hierarchical porous structure with abundant surface microporous structure to host the active sites should help further increase the mass activity; (2) mitigating the mass transfer issues of the Fe/N/C-based MEA because of the thick catalyst layer, for example, building an effective three-phase boundary; and (3) improving the durability from the perspective of catalysts and engineering design.

At last, standard procedures for the evaluation of Fe/N/C electrocatalysts should be established on both RDEs and MEAs. Currently, the evaluation of the activity and the stability of the catalysts are not conducted under the same protocols among different research groups. For example, the stability of the MEA is either evaluated through the chronoamperometry method under different cell potentials or tested by cycling potential with different cycles. These inconsistent testing protocols prevent comparison and cooperation among different laboratories. A unified test protocol should be established to effectively push the limits of the Fe/N/C based PEMFCs.

AUTHOR INFORMATION

Corresponding Authors

*Email: q.jia@northeastern.edu.
*Email: s.mukerjee@northeastern.edu.
*Email: slchen@whu.edu.cn.

ORCID

Sanjeev Mukerjee: 0000-0002-2980-7655
Shengli Chen: 0000-0001-7448-8860

Notes

The authors declare no competing financial interest.

ACKNOWLEDGMENTS

This work was supported by the Natural Science Foundation of China (Grant Nos. 21832004 and 21633008). As a joint Ph.D. candidate in Northeastern University, Wang Wang was also supported by a fellowship from the China Scholarship Council.

REFERENCES

(1) Seh, Z. W.; Kibsgaard, J.; Dickens, C. F.; Chorkendorff, I.; Nørskov, J. K.; Jaramillo, T. F. Combining Theory and Experiment in Electrocatalysis: Insights into Materials Design. *Science* **2017**, *355*, No. eaad4998.

(2) Zhao, Y.; Wan, J.; Yao, H.; Zhang, L.; Lin, K.; Wang, L.; Yang, N.; Liu, D.; Song, L.; Zhu, J.; Gu, L.; Liu, L.; Zhao, H.; Li, Y.; Wang, D. Few-Layer Graphdiyne Doped with Sp-Hybridized Nitrogen Atoms at Acetylenic Sites for Oxygen Reduction Electrocatalysis. *Nat. Chem.* **2018**, *10*, 924−931.

(3) Liu, J.; Jiao, M.; Lu, L.; Barkholtz, H. M.; Li, Y.; Wang, Y.; Jiang, L.; Wu, Z.; Liu, D.-j.; Zhuang, L.; Ma, C.; Zeng, J.; Zhang, B.; Su, D.; Song, P.; Xing, W.; Xu, W.; Wang, Y.; Jiang, Z.; Sun, G. High Performance Platinum Single Atom Electrocatalyst for Oxygen Reduction Reaction. *Nat. Commun.* **2017**, *8*, 15938.

(4) Zhang, W.; Lai, W.; Cao, R. Energy-Related Small Molecule Activation Reactions: Oxygen Reduction and Hydrogen and Oxygen Evolution Reactions Catalyzed by Porphyrin- and Corrole-Based Systems. *Chem. Rev.* **2017**, *117*, 3717−3797.

(5) Zheng, Y.; Jiao, Y.; Qiao, S. Z. Engineering of Carbon-Based Electrocatalysts for Emerging Energy Conversion: From Fundamentality to Functionality. *Adv. Mater.* **2015**, *27*, 5372−5378.

(6) Wang, W.; Hu, Y.; Liu, Y.; Zheng, Z.; Chen, S. Self-Powered and Highly Efficient Production of H2o2 through a Zn−Air Battery with Oxygenated Carbon Electrocatalyst. *ACS Appl. Mater. Interfaces* **2018**, *10*, 31855−31859.

(7) Lee, J.-S.; Tai Kim, S.; Cao, R.; Choi, N.-S.; Liu, M.; Lee, K. T.; Cho, J. Metal−Air Batteries with High Energy Density: Li−Air Versus Zn−Air. *Adv. Energy. Mater.* **2011**, *1*, 34−50.

(8) Wang, H.-F.; Tang, C.; Zhang, Q. A Review of Precious-Metal-Free Bifunctional Oxygen Electrocatalysts: Rational Design and Applications in Zn−Air Batteries. *Adv. Funct. Mater.* **2018**, *28*, 1803329.

(9) Li, M.; Zhao, Z.; Cheng, T.; Fortunelli, A.; Chen, C.-Y.; Yu, R.; Zhang, Q.; Gu, L.; Merinov, B. V.; Lin, Z.; Zhu, E.; Yu, T.; Jia, Q.; Guo, J.; Zhang, L.; Goddard, W. A.; Huang, Y.; Duan, X. Ultrafine Jagged Platinum Nanowires Enable Ultrahigh Mass Activity for the Oxygen Reduction Reaction. *Science* **2016**, *354*, 1414−1419.

(10) Bu, L.; Zhang, N.; Guo, S.; Zhang, X.; Li, J.; Yao, J.; Wu, T.; Lu, G.; Ma, J.-Y.; Su, D.; Huang, X. Biaxially Strained Ptpb/Pt Core/Shell Nanoplate Boosts Oxygen Reduction Catalysis. *Science* **2016**, *354*, 1410−1414.

(11) Lv, H.; Li, D.; Strmcnik, D.; Paulikas, A. P.; Markovic, N. M.; Stamenkovic, V. R. Recent Advances in the Design of Tailored Nanomaterials for Efficient Oxygen Reduction Reaction. *Nano Energy* **2016**, *29*, 149−165.

(12) Wang, C.; Markovic, N. M.; Stamenkovic, V. R. Advanced Platinum Alloy Electrocatalysts for the Oxygen Reduction Reaction. *ACS Catal.* **2012**, *2*, 891−898.

(13) U.S. Department of Energy, T. P. F. C., 2012, https://www.energy.gov/sites/prod/files/2014/12/f19/fcto_myrdd_full_document.pdf.

DOI: 10.1021/acscatal.9b02583
ACS Catal. 2019, 9, 10126−10141

(14) U.S. Department of Energy, T. P. F. C., 2017, https://www.energy.gov/sites/prod/files/2017/11/f46/FCTT_Roadmap_Nov_2017_FINAL.pdf.
(15) Steinbach, A. Final Report - High Performance, Durable, Low Cost Membrane Electrode Assemblies for Transportation Applications; United States, 2017-05-31, 2017.
(16) Nie, Y.; Li, L.; Wei, Z. Recent Advancements in Pt and Pt-Free Catalysts for Oxygen Reduction Reaction. *Chem. Soc. Rev.* **2015**, *44*, 2168−2201.
(17) Xia, W.; Mahmood, A.; Liang, Z.; Zou, R.; Guo, S. Earth-Abundant Nanomaterials for Oxygen Reduction. *Angew. Chem., Int. Ed.* **2016**, *55*, 2650−2676.
(18) Wang, Y.-J.; Wilkinson, D. P.; Zhang, J. Noncarbon Support Materials for Polymer Electrolyte Membrane Fuel Cell Electrocatalysts. *Chem. Rev.* **2011**, *111*, 7625−7651.
(19) Zhou, X.; Qiao, J.; Yang, L.; Zhang, J. A Review of Graphene-Based Nanostructural Materials for Both Catalyst Supports and Metal-Free Catalysts in Pem Fuel Cell Oxygen Reduction Reactions. *Adv. Energy. Mater.* **2014**, *4*, 1301523.
(20) Cheng, X.; Shi, Z.; Glass, N.; Zhang, L.; Zhang, J.; Song, D.; Liu, Z.-S.; Wang, H.; Shen, J. A Review of Pem Hydrogen Fuel Cell Contamination: Impacts, Mechanisms, and Mitigation. *J. Power Sources* **2007**, *165*, 739−756.
(21) Baschuk, J. J.; Li, X. Carbon Monoxide Poisoning of Proton Exchange Membrane Fuel Cells. *Int. J. Energy Res.* **2001**, *25*, 695−713.
(22) Jasinski, R. A New Fuel Cell Cathode Catalyst. *Nature* **1964**, *201*, 1212.
(23) Gupta, S.; Tryk, D.; Bae, I.; Aldred, W.; Yeager, E. Heat-Treated Polyacrylonitrile-Based Catalysts for Oxygen Electroreduction. *J. Appl. Electrochem.* **1989**, *19*, 19−27.
(24) Jahnke, H.; Schönborn, M.; Zimmermann, G. Organic Dyestuffs as Catalysts for Fuel Cells, *Physical and Chemical Applications of Dyestuffs*; Springer, 1976; pp 133−181.
(25) Bezerra, C. W. B.; Zhang, L.; Lee, K.; Liu, H.; Marques, A. L. B.; Marques, E. P.; Wang, H.; Zhang, J. A Review of Fe−N/C and Co−N/C Catalysts for the Oxygen Reduction Reaction. *Electrochim. Acta* **2008**, *53*, 4937−4951.
(26) Raj, C. R.; Samanta, A.; Noh, S. H.; Mondal, S.; Okajima, T.; Ohsaka, T. Emerging New Generation Electrocatalysts for the Oxygen Reduction Reaction. *J. Mater. Chem. A* **2016**, *4*, 11156−11178.
(27) Zhu, C.; Li, H.; Fu, S.; Du, D.; Lin, Y. Highly Efficient Nonprecious Metal Catalysts Towards Oxygen Reduction Reaction Based on Three-Dimensional Porous Carbon Nanostructures. *Chem. Soc. Rev.* **2016**, *45*, 517−531.
(28) Jaouen, F.; Herranz, J.; Lefèvre, M.; Dodelet, J.-P.; Kramm, U. I.; Herrmann, I.; Bogdanoff, P.; Maruyama, J.; Nagaoka, T.; Garsuch, A.; Dahn, J. R.; Olson, T.; Pylypenko, S.; Atanassov, P.; Ustinov, E. A. Cross-Laboratory Experimental Study of Non-Noble-Metal Electrocatalysts for the Oxygen Reduction Reaction. *ACS Appl. Mater. Interfaces* **2009**, *1*, 1623−1639.
(29) Gojković, S. L.; Gupta, S.; Savinell, R. F. Heat-Treated Iron(Iii) Tetramethoxyphenyl Porphyrin Chloride Supported on High-Area Carbon as an Electrocatalyst for Oxygen Reduction: Part Ii. Kinetics of Oxygen Reduction. *J. Electroanal. Chem.* **1999**, *462*, 63−72.
(30) Sun, G. Q.; Wang, J. T.; Gupta, S.; Savinell, R. F. Iron(Iii) Tetramethoxyphenylporphyrin (Fetmpp-C1) as Electrocatalyst for Oxygen Reduction in Direct Methanol Fuel Cells. *J. Appl. Electrochem.* **2001**, *31*, 1025−1031.
(31) Lalande, G.; Côté, R.; Guay, D.; Dodelet, J. P.; Weng, L. T.; Bertrand, P. Is Nitrogen Important in the Formulation of Fe-Based Catalysts for Oxygen Reduction in Solid Polymer Fuel Cells? *Electrochim. Acta* **1997**, *42*, 1379−1388.
(32) Gouérec, P.; Savy, M.; Riga, J. Oxygen Reduction in Acidic Media Catalyzed by Pyrolyzed Cobalt Macrocycles Dispersed on an Active Carbon: The Importance of the Content of Oxygen Surface Groups on the Evolution of the Chelate Structure During the Heat Treatment. *Electrochim. Acta* **1998**, *43*, 743−753.
(33) Ferrandon, M.; Kropf, A. J.; Myers, D. J.; Artyushkova, K.; Kramm, U.; Bogdanoff, P.; Wu, G.; Johnston, C. M.; Zelenay, P. Multitechnique Characterization of a Polyaniline−Iron−Carbon Oxygen Reduction Catalyst. *J. Phys. Chem. C* **2012**, *116*, 16001−16013.
(34) Jia, Q.; Liu, E.; Jiao, L.; Pann, S.; Mukerjee, S. X-Ray Absorption Spectroscopy Characterizations on Pgm-Free Electrocatalysts: Justification, Advantages, and Limitations. *Adv. Mater.* **2019**, *31*, 1805157.
(35) Jaouen, F.; Serventi, A. M.; Lefèvre, M.; Dodelet, J.-P.; Bertrand, P. Non-Noble Electrocatalysts for O2 Reduction: How Does Heat Treatment Affect Their Activity and Structure? Part Ii. Structural Changes Observed by Electron Microscopy, Raman, and Mass Spectroscopy. *J. Phys. Chem. C* **2007**, *111*, 5971−5976.
(36) Zhang, S.; Zhang, H.; Liu, Q.; Chen, S. Fe−N Doped Carbon Nanotube/Graphene Composite: Facile Synthesis and Superior Electrocatalytic Activity. *J. Mater. Chem. A* **2013**, *1*, 3302−3308.
(37) Kramm, U. I.; Ni, L.; Wagner, S. 57fe Mössbauer Spectroscopy Characterization of Electrocatalysts. *Adv. Mater.* **2019**, *31*, 1805623.
(38) Liu, K.; Wu, G.; Wang, G. Role of Local Carbon Structure Surrounding Fen4 Sites in Boosting the Catalytic Activity for Oxygen Reduction. *J. Phys. Chem. C* **2017**, *121*, 11319−11324.
(39) Kramm, U. I.; Herrmann-Geppert, I.; Behrends, J.; Lips, K.; Fiechter, S.; Bogdanoff, P. On an Easy Way to Prepare Metal−Nitrogen Doped Carbon with Exclusive Presence of Men4-Type Sites Active for the Orr. *J. Am. Chem. Soc.* **2016**, *138*, 635−640.
(40) He, W.; Wang, Y.; Jiang, C.; Lu, L. Structural Effects of a Carbon Matrix in Non-Precious Metal O2-Reduction Electrocatalysts. *Chem. Soc. Rev.* **2016**, *45*, 2396−2409.
(41) Shao, M.; Chang, Q.; Dodelet, J.-P.; Chenitz, R. Recent Advances in Electrocatalysts for Oxygen Reduction Reaction. *Chem. Rev.* **2016**, *116*, 3594−3657.
(42) Jiao, Y.; Zheng, Y.; Jaroniec, M.; Qiao, S. Z. Design of Electrocatalysts for Oxygen- and Hydrogen-Involving Energy Conversion Reactions. *Chem. Soc. Rev.* **2015**, *44*, 2060−2086.
(43) Hong, W. T.; Risch, M.; Stoerzinger, K. A.; Grimaud, A.; Suntivich, J.; Shao-Horn, Y. Toward the Rational Design of Non-Precious Transition Metal Oxides for Oxygen Electrocatalysis. *Energy Environ. Sci.* **2015**, *8*, 1404−1427.
(44) Artyushkova, K.; Serov, A.; Rojas-Carbonell, S.; Atanassov, P. Chemistry of Multitudinous Active Sites for Oxygen Reduction Reaction in Transition Metal−Nitrogen−Carbon Electrocatalysts. *J. Phys. Chem. C* **2015**, *119*, 25917−25928.
(45) Choi, C. H.; Choi, W. S.; Kasian, O.; Mechler, A. K.; Sougrati, M. T.; Brüller, S.; Strickland, K.; Jia, Q.; Mukerjee, S.; Mayrhofer, K. J. J.; Jaouen, F. Unraveling the Nature of Sites Active toward Hydrogen Peroxide Reduction in Fe-N-C Catalysts. *Angew. Chem., Int. Ed.* **2017**, *56*, 8809−8812.
(46) Zitolo, A.; Goellner, V.; Armel, V.; Sougrati, M.-T.; Mineva, T.; Stievano, L.; Fonda, E.; Jaouen, F. Identification of Catalytic Sites for Oxygen Reduction in Iron- and Nitrogen-Doped Graphene materials. *Nat. Mater.* **2015**, *14*, 937.
(47) Tylus, U.; Jia, Q.; Strickland, K.; Ramaswamy, N.; Serov, A.; Atanassov, P.; Mukerjee, S. Elucidating Oxygen Reduction Active Sites in Pyrolyzed Metal−Nitrogen Coordinated Non-Precious-Metal Electrocatalyst Systems. *J. Phys. Chem. C* **2014**, *118*, 8999−9008.
(48) Kattel, S.; Wang, G. Reaction Pathway for Oxygen Reduction on FeN_4 Embedded Graphene. *J. Phys. Chem. Lett.* **2014**, *5*, 452−456.
(49) Guo, D.; Shibuya, R.; Akiba, C.; Saji, S.; Kondo, T.; Nakamura, J. Active Sites of Nitrogen-Doped Carbon Materials for Oxygen Reduction Reaction Clarified Using Model Catalysts. *Science* **2016**, *351*, 361−365.
(50) Subramanian, N. P.; Li, X.; Nallathambi, V.; Kumaraguru, S. P.; Colon-Mercado, H.; Wu, G.; Lee, J.-W.; Popov, B. N. Nitrogen-Modified Carbon-Based Catalysts for Oxygen Reduction Reaction in Polymer Electrolyte Membrane Fuel Cells. *J. Power Sources* **2009**, *188*, 38−44.
(51) Rao, C. V.; Cabrera, C. R.; Ishikawa, Y. In Search of the Active Site in Nitrogen-Doped Carbon Nanotube Electrodes for the Oxygen Reduction Reaction. *J. Phys. Chem. Lett.* **2010**, *1*, 2622−2627.

DOI: 10.1021/acscatal.9b02583
ACS Catal. 2019, 9, 10126−10141

(52) Strickland, K.; Miner, E.; Jia, Q.; Tylus, U.; Ramaswamy, N.; Liang, W.; Sougrati, M.-T.; Jaouen, F.; Mukerjee, S. Highly Active Oxygen Reduction Non-Platinum Group Metal Electrocatalyst without Direct Metal−Nitrogen Coordination. *Nat. Commun.* **2015**, *6*, 7343.
(53) Varnell, J. A.; Sotiropoulos, J. S.; Brown, T. M.; Subedi, K.; Haasch, R. T.; Schulz, C. E.; Gewirth, A. A. Revealing the Role of the Metal in Non-Precious-Metal Catalysts for Oxygen Reduction Via Selective Removal of Fe. *ACS Energy Lett.* **2018**, *3*, 823−828.
(54) Masa, J.; Xia, W.; Muhler, M.; Schuhmann, W. On the Role of Metals in Nitrogen-Doped Carbon Electrocatalysts for Oxygen Reduction. *Angew. Chem., Int. Ed.* **2015**, *54*, 10102−10120.
(55) Wang, P.; Ma, Z.; Zhao, Z.; Jia, L. Oxygen Reduction on the Electrocatalysts Based on Pyrolyzed Non-Noble Metal/Poly-O-Phenylenediamine/Carbon Black Composites: New Insight into the Active Sites. *J. Electroanal. Chem.* **2007**, *611*, 87−95.
(56) Matter, P. H.; Wang, E.; Millet, J.-M. M.; Ozkan, U. S. Characterization of the Iron Phase in Cnx-Based Oxygen Reduction Reaction Catalysts. *J. Phys. Chem. C* **2007**, *111*, 1444−1450.
(57) Gouérec, P.; Savy, M. Oxygen Reduction Electrocatalysis: Ageing of Pyrolyzed Cobalt Macrocycles Dispersed on an Active Carbon. *Electrochim. Acta* **1999**, *44*, 2653−2661.
(58) Maldonado, S.; Stevenson, K. J. Influence of Nitrogen Doping on Oxygen Reduction Electrocatalysis at Carbon Nanofiber Electrodes. *J. Phys. Chem. B* **2005**, *109*, 4707−4716.
(59) Franke, R.; Ohms, D.; Wiesener, K. Investigation of the Influence of Thermal Treatment on the Properties of Carbon Materials Modified by N4-Chelates for the Reduction of Oxygen in Acidic Media. *J. Electroanal. Chem. Interfacial Electrochem.* **1989**, *260*, 63−73.
(60) Singh, D.; Mamtani, K.; Bruening, C. R.; Miller, J. T.; Ozkan, U. S. Use of H2s to Probe the Active Sites in Fenc Catalysts for the Oxygen Reduction Reaction (Orr) in Acidic Media. *ACS Catal.* **2014**, *4*, 3454−3462.
(61) Zhang, J.; Dai, L. Heteroatom-Doped Graphitic Carbon Catalysts for Efficient Electrocatalysis of Oxygen Reduction Reaction. *ACS Catal.* **2015**, *5*, 7244−7253.
(62) Workman, M. J.; Serov, A.; Tsui, L.-k.; Atanassov, P.; Artyushkova, K. Fe−N−C Catalyst Graphitic Layer Structure and Fuel Cell Performance. *ACS Energy Lett.* **2017**, *2*, 1489−1493.
(63) Lefèvre, M.; Dodelet, J. P.; Bertrand, P. Molecular Oxygen Reduction in Pem Fuel Cells: Evidence for the Simultaneous Presence of Two Active Sites in Fe-Based Catalysts. *J. Phys. Chem. B* **2002**, *106*, 8705−8713.
(64) Kabir, S.; Artyushkova, K.; Kiefer, B.; Atanassov, P. Computational and Experimental Evidence for a New Tm−N3/C Moiety Family in Non-Pgm Electrocatalysts. *Phys. Chem. Chem. Phys.* **2015**, *17*, 17785−17789.
(65) Jia, Q.; Ramaswamy, N.; Tylus, U.; Strickland, K.; Li, J.; Serov, A.; Artyushkova, K.; Atanassov, P.; Anibal, J.; Gumeci, C.; Barton, S. C.; Sougrati, M.-T.; Jaouen, F.; Halevi, B.; Mukerjee, S. Spectroscopic Insights into the Nature of Active Sites in Iron−Nitrogen−Carbon Electrocatalysts for Oxygen Reduction in Acid. *Nano Energy* **2016**, *29*, 65−82.
(66) Chong, L.; Wen, J.; Kubal, J.; Sen, F. G.; Zou, J.; Greeley, J.; Chan, M.; Barkholtz, H.; Ding, W.; Liu, D.-J. Ultralow-Loading Platinum-Cobalt Fuel Cell Catalysts Derived from Imidazolate Frameworks. *Science* **2018**, *362*, 1276−1281.
(67) Chung, H. T.; Cullen, D. A.; Higgins, D.; Sneed, B. T.; Holby, E. F.; More, K. L.; Zelenay, P. Direct Atomic-Level Insight into the Active Sites of a High-Performance PGM-Free ORR Catalyst. *Science* **2017**, *357*, 479−484.
(68) Fei, H.; Dong, J.; Feng, Y.; Allen, C. S.; Wan, C.; Volosskiy, B.; Li, M.; Zhao, Z.; Wang, Y.; Sun, H.; An, P.; Chen, W.; Guo, Z.; Lee, C.; Chen, D.; Shakir, I.; Liu, M.; Hu, T.; Li, Y.; Kirkland, A. I.; Duan, X.; Huang, Y. General Synthesis and Definitive Structural Identification of Mn4C4 Single-Atom Catalysts with Tunable Electrocatalytic Activities. *Nat. Catal.* **2018**, *1*, 63−72.
(69) Bouwkamp-Wijnoltz, A. L.; Visscher, W.; van Veen, J. A. R.; Boellaard, E.; van der Kraan, A. M.; Tang, S. C. On Active-Site Heterogeneity in Pyrolyzed Carbon-Supported Iron Porphyrin Catalysts for the Electrochemical Reduction of Oxygen: An in Situ Mössbauer Study. *J. Phys. Chem. B* **2002**, *106*, 12993−13001.
(70) Calle-Vallejo, F.; Martínez, J. I.; Rossmeisl, J. Density Functional Studies of Functionalized Graphitic Materials with Late Transition Metals for Oxygen Reduction Reactions. *Phys. Chem. Chem. Phys.* **2011**, *13*, 15639−15643.
(71) Kramm, U. I.; Abs-Wurmbach, I.; Herrmann-Geppert, I.; Radnik, J.; Fiechter, S.; Bogdanoff, P. Influence of the Electron-Density of FeN4-Centers Towards the Catalytic Activity of Pyrolyzed FeTMPPCl-Based ORR-Electrocatalysts. *J. Electrochem. Soc.* **2011**, *158*, B69−B78.
(72) Ramaswamy, N.; Tylus, U.; Jia, Q.; Mukerjee, S. Activity Descriptor Identification for Oxygen Reduction on Nonprecious Electrocatalysts: Linking Surface Science to Coordination Chemistry. *J. Am. Chem. Soc.* **2013**, *135*, 15443−15449.
(73) Jiang, W.-J.; Gu, L.; Li, L.; Zhang, Y.; Zhang, X.; Zhang, L.-J.; Wang, J.-Q.; Hu, J.-S.; Wei, Z.; Wan, L.-J. Understanding the High Activity of Fe−N−C Electrocatalysts in Oxygen Reduction: Fe/Fe3c Nanoparticles Boost the Activity of Fe−Nx. *J. Am. Chem. Soc.* **2016**, *138*, 3570−3578.
(74) Yang, L.; Cheng, D.; Xu, H.; Zeng, X.; Wan, X.; Shui, J.; Xiang, Z.; Cao, D. Unveiling the High-Activity Origin of Single-Atom Iron Catalysts for Oxygen Reduction Reaction. *Proc. Natl. Acad. Sci. U. S. A.* **2018**, *115*, 6626.
(75) Kramm, U. I.; Herranz, J.; Larouche, N.; Arruda, T. M.; Lefèvre, M.; Jaouen, F.; Bogdanoff, P.; Fiechter, S.; Abs-Wurmbach, I.; Mukerjee, S.; Dodelet, J.-P. Structure of the Catalytic Sites in Fe/N/C-Catalysts for O2-Reduction in Pem Fuel Cells. *Phys. Chem. Chem. Phys.* **2012**, *14*, 11673−11688.
(76) Kramm, U. I.; Lefèvre, M.; Larouche, N.; Schmeisser, D.; Dodelet, J.-P. Correlations between Mass Activity and Physicochemical Properties of Fe/N/C Catalysts for the Orr in Pem Fuel Cell Via 57fe Mössbauer Spectroscopy and Other Techniques. *J. Am. Chem. Soc.* **2014**, *136*, 978−985.
(77) Liang, W.; Chen, J.; Liu, Y.; Chen, S. Density-Functional-Theory Calculation Analysis of Active Sites for Four-Electron Reduction of O2 on Fe/N-Doped Graphene. *ACS Catal.* **2014**, *4*, 4170−4177.
(78) Sougrati, M. T.; Goellner, V.; Schuppert, A. K.; Stievano, L.; Jaouen, F. Probing Active Sites in Iron-Based Catalysts for Oxygen Electro-Reduction: A Temperature-Dependent 57fe Mössbauer Spectroscopy Study. *Catal. Today* **2016**, *262*, 110−120.
(79) Jia, Q.; Ramaswamy, N.; Hafiz, H.; Tylus, U.; Strickland, K.; Wu, G.; Barbiellini, B.; Bansil, A.; Holby, E. F.; Zelenay, P.; Mukerjee, S. Experimental Observation of Redox-Induced Fe−N Switching Behavior as a Determinant Role for Oxygen Reduction Activity. *ACS Nano* **2015**, *9*, 12496−12505.
(80) Li, J.; Jaouen, F. Structure and Activity of Metal-Centered Coordination Sites in Pyrolyzed Metal−Nitrogen−Carbon Catalysts for the Electrochemical Reduction of O2. *Curr. Opin. Electrochem.* **2018**, *9*, 198−206.
(81) Li, J.; Ghoshal, S.; Liang, W.; Sougrati, M.-T.; Jaouen, F.; Halevi, B.; McKinney, S.; McCool, G.; Ma, C.; Yuan, X.; Ma, Z.-F.; Mukerjee, S.; Jia, Q. Structural and Mechanistic Basis for the High Activity of Fe−N−C Catalysts toward Oxygen Reduction. *Energy Environ. Sci.* **2016**, *9*, 2418−2432.
(82) Xiao, M.; Zhu, J.; Ma, L.; Jin, Z.; Ge, J.; Deng, X.; Hou, Y.; He, Q.; Li, J.; Jia, Q.; Mukerjee, S.; Yang, R.; Jiang, Z.; Su, D.; Liu, C.; Xing, W. Microporous Framework Induced Synthesis of Single-Atom Dispersed Fe-N-C Acidic Orr Catalyst and Its in Situ Reduced Fe-N4 Active Site Identification Revealed by X-Ray Absorption Spectroscopy. *ACS Catal.* **2018**, *8*, 2824−2832.
(83) Wang, Y.-C.; Lai, Y.-J.; Song, L.; Zhou, Z.-Y.; Liu, J.-G.; Wang, Q.; Yang, X.-D.; Chen, C.; Shi, W.; Zheng, Y.-P.; Rauf, M.; Sun, S.-G. S-Doping of an Fe/N/C Orr Catalyst for Polymer Electrolyte

DOI: 10.1021/acscatal.9b02583
ACS Catal. 2019, 9, 10126−10141

Membrane Fuel Cells with High Power Density. *Angew. Chem.* **2015**, *127*, 10045−10048.
(84) Birry, L.; Zagal, J. H.; Dodelet, J.-P. Does Co Poison Fe-Based Catalysts for Orr? *Electrochem. Commun.* **2010**, *12*, 628−631.
(85) Koslowski, U. I.; Abs-Wurmbach, I.; Fiechter, S.; Bogdanoff, P. Nature of the Catalytic Centers of Porphyrin-Based Electrocatalysts for the Orr: A Correlation of Kinetic Current Density with the Site Density of Fe−N4 Centers. *J. Phys. Chem. C* **2008**, *112*, 15356−15366.
(86) Jaouen, F.; Dodelet, J.-P. Average Turn-over Frequency of O2 Electro-Reduction for Fe/N/C and Co/N/C Catalysts in Pefcs. *Electrochim. Acta* **2007**, *52*, 5975−5984.
(87) Sahraie, N. R.; Kramm, U. I.; Steinberg, J.; Zhang, Y.; Thomas, A.; Reier, T.; Paraknowitsch, J.-P.; Strasser, P. Quantifying the Density and Utilization of Active Sites in Non-Precious Metal Oxygen Electroreduction Catalysts. *Nat. Commun.* **2015**, *6*, 8618.
(88) Malko, D.; Kucernak, A.; Lopes, T. In Situ Electrochemical Quantification of Active Sites in Fe−N/C Non-Precious Metal Catalysts. *Nat. Commun.* **2016**, *7*, 13285.
(89) Lefèvre, M.; Dodelet, J. P.; Bertrand, P. O2 Reduction in Pem Fuel Cells: Activity and Active Site Structural Information for Catalysts Obtained by the Pyrolysis at High Temperature of Fe Precursors. *J. Phys. Chem. B* **2000**, *104*, 11238−11247.
(90) Wu, G.; Chen, Z.; Artyushkova, K.; Garzon, F. H.; Zelenay, P. Polyaniline-Derived Non-Precious Catalyst for the Polymer Electrolyte Fuel Cell Cathode. *ECS Trans.* **2008**, *16*, 159−170.
(91) Wang, D.-W.; Su, D. Heterogeneous Nanocarbon Materials for Oxygen Reduction Reaction. *Energy Environ. Sci.* **2014**, *7*, 576−591.
(92) Yang, N.; Li, L.; Li, J.; Ding, W.; Wei, Z. Modulating the Oxygen Reduction Activity of Heteroatom-Doped Carbon Catalysts Via the Triple Effect: Charge, Spin Density and Ligand Effect. *Chem. Sci.* **2018**, *9*, 5795−5804.
(93) Zhao, Z.; Li, M.; Zhang, L.; Dai, L.; Xia, Z. Design Principles for Heteroatom-Doped Carbon Nanomaterials as Highly Efficient Catalysts for Fuel Cells and Metal−Air Batteries. *Adv. Mater.* **2015**, *27*, 6834−6840.
(94) Zhang, L.; Xia, Z. Mechanisms of Oxygen Reduction Reaction on Nitrogen-Doped Graphene for Fuel Cells. *J. Phys. Chem. C* **2011**, *115*, 11170−11176.
(95) Hu, X.; Wu, Y.; Li, H.; Zhang, Z. Adsorption and Activation of O2 on Nitrogen-Doped Carbon Nanotubes. *J. Phys. Chem. C* **2010**, *114*, 9603−9607.
(96) Wei, D.; Liu, Y.; Wang, Y.; Zhang, H.; Huang, L.; Yu, G. Synthesis of N-Doped Graphene by Chemical Vapor Deposition and Its Electrical Properties. *Nano Lett.* **2009**, *9*, 1752−1758.
(97) Lai, L.; Potts, J. R.; Zhan, D.; Wang, L.; Poh, C. K.; Tang, C.; Gong, H.; Shen, Z.; Lin, J.; Ruoff, R. S. Exploration of the Active Center Structure of Nitrogen-Doped Graphene-Based Catalysts for Oxygen Reduction Reaction. *Energy Environ. Sci.* **2012**, *5*, 7936−7942.
(98) Niwa, H.; Horiba, K.; Harada, Y.; Oshima, M.; Ikeda, T.; Terakura, K.; Ozaki, J.-i.; Miyata, S. X-Ray Absorption Analysis of Nitrogen Contribution to Oxygen Reduction Reaction in Carbon Alloy Cathode Catalysts for Polymer Electrolyte Fuel Cells. *J. Power Sources* **2009**, *187*, 93−97.
(99) Ding, W.; Wei, Z.; Chen, S.; Qi, X.; Yang, T.; Hu, J.; Wang, D.; Wan, L.-J.; Alvi, S. F.; Li, L. Space-Confinement-Induced Synthesis of Pyridinic- and Pyrrolic-Nitrogen-Doped Graphene for the Catalysis of Oxygen Reduction. *Angew. Chem.* **2013**, *125*, 11971−11975.
(100) Xing, T.; Zheng, Y.; Li, L. H.; Cowie, B. C. C.; Gunzelmann, D.; Qiao, S. Z.; Huang, S.; Chen, Y. Observation of Active Sites for Oxygen Reduction Reaction on Nitrogen-Doped Multilayer Graphene. *ACS Nano* **2014**, *8*, 6856−6862.
(101) Kim, H.; Lee, K.; Woo, S. I.; Jung, Y. On the Mechanism of Enhanced Oxygen Reduction Reaction in Nitrogen-Doped Graphene Nanoribbons. *Phys. Chem. Chem. Phys.* **2011**, *13*, 17505−17510.
(102) Dodelet, J.-P.; Chenitz, R.; Yang, L.; Lefèvre, M. A New Catalytic Site for the Electroreduction of Oxygen? *ChemCatChem* **2014**, *6*, 1866−1867.
(103) Chung, H. T.; Won, J. H.; Zelenay, P. Active and Stable Carbon Nanotube/Nanoparticle Composite Electrocatalyst for Oxygen Reduction. *Nat. Commun.* **2013**, *4*, 1922.
(104) Wen, Z.; Ci, S.; Zhang, F.; Feng, X.; Cui, S.; Mao, S.; Luo, S.; He, Z.; Chen, J. Nitrogen-Enriched Core-Shell Structured Fe/Fe3c-C Nanorods as Advanced Electrocatalysts for Oxygen Reduction Reaction. *Adv. Mater.* **2012**, *24*, 1399−1404.
(105) Hu, Y.; Jensen, J. O.; Zhang, W.; Cleemann, L. N.; Xing, W.; Bjerrum, N. J.; Li, Q. Hollow Spheres of Iron Carbide Nanoparticles Encased in Graphitic Layers as Oxygen Reduction Catalysts. *Angew. Chem., Int. Ed.* **2014**, *53*, 3675−3679.
(106) Deng, D.; Yu, L.; Chen, X.; Wang, G.; Jin, L.; Pan, X.; Deng, J.; Sun, G.; Bao, X. Iron Encapsulated within Pod-Like Carbon Nanotubes for Oxygen Reduction Reaction. *Angew. Chem., Int. Ed.* **2013**, *52*, 371−375.
(107) Meng, H.; Jaouen, F.; Proietti, E.; Lefèvre, M.; Dodelet, J.-P. Ph-Effect on Oxygen Reduction Activity of Fe-Based Electrocatalysts. *Electrochem. Commun.* **2009**, *11*, 1986−1989.
(108) Ramaswamy, N.; Mukerjee, S. Influence of Inner- and Outer-Sphere Electron Transfer Mechanisms During Electrocatalysis of Oxygen Reduction in Alkaline Media. *J. Phys. Chem. C* **2011**, *115*, 18015−18026.
(109) Ramaswamy, N.; Mukerjee, S. Fundamental Mechanistic Understanding of Electrocatalysis of Oxygen Reduction on Pt and Non-Pt Surfaces: Acid Versus Alkaline Media. *Adv. Phys. Chem.* **2012**, *2012*, 491604.
(110) Wang, W.; Chen, W.; Miao, P.; Luo, J.; Wei, Z.; Chen, S. Nacl Crystallites as Dual-Functional and Water-Removable Templates to Synthesize a Three-Dimensional Graphene-Like Macroporous Fe-N-C Catalyst. *ACS Catal.* **2017**, *7*, 6144−6149.
(111) Lin, L.; Zhu, Q.; Xu, A.-W. Noble-Metal-Free Fe−N/C Catalyst for Highly Efficient Oxygen Reduction Reaction under Both Alkaline and Acidic Conditions. *J. Am. Chem. Soc.* **2014**, *136*, 11027−11033.
(112) Wan, K.; Yu, Z.-p.; Li, X.-h.; Liu, M.-y.; Yang, G.; Piao, J.-h.; Liang, Z.-x. Ph Effect on Electrochemistry of Nitrogen-Doped Carbon Catalyst for Oxygen Reduction Reaction. *ACS Catal.* **2015**, *5*, 4325−4332.
(113) Liu, G.; Li, X.; Ganesan, P.; Popov, B. N. Studies of Oxygen Reduction Reaction Active Sites and Stability of Nitrogen-Modified Carbon Composite Catalysts for Pem Fuel Cells. *Electrochim. Acta* **2010**, *55*, 2853−2858.
(114) Herranz, J.; Jaouen, F.; Lefèvre, M.; Kramm, U. I.; Proietti, E.; Dodelet, J.-P.; Bogdanoff, P.; Fiechter, S.; Abs-Wurmbach, I.; Bertrand, P.; Arruda, T. M.; Mukerjee, S. Unveiling N-Protonation and Anion-Binding Effects on Fe/N/C Catalysts for O2 Reduction in Proton-Exchange-Membrane Fuel Cells. *J. Phys. Chem. C* **2011**, *115*, 16087−16097.
(115) Rauf, M.; Zhao, Y.-D.; Wang, Y.-C.; Zheng, Y.-P.; Chen, C.; Yang, X.-D.; Zhou, Z.-Y.; Sun, S.-G. Insight into the Different ORR Catalytic Activity of Fe/N/C between Acidic and Alkaline Media: Protonation of Pyridinic Nitrogen. *Electrochem. Commun.* **2016**, *73*, 71−74.
(116) Zhang, H.; Chung, H. T.; Cullen, D. A.; Wagner, S.; Kramm, U. I.; More, K. L.; Zelenay, P.; Wu, G. High-Performance Fuel Cell Cathodes Exclusively Containing Atomically Dispersed Iron Active Sites. *Energy Environ. Sci.* **2019**, *12*, 2548−2558.
(117) Choi, J.-Y.; Yang, L.; Kishimoto, T.; Fu, X.; Ye, S.; Chen, Z.; Banham, D. Is the Rapid Initial Performance Loss of Fe/N/C Non Precious Metal Catalysts Due to Micropore Flooding? *Energy Environ. Sci.* **2017**, *10*, 296−305.
(118) Proietti, E.; Jaouen, F.; Lefèvre, M.; Larouche, N.; Tian, J.; Herranz, J.; Dodelet, J.-P. Iron-Based Cathode Catalyst with Enhanced Power Density in Polymer Electrolyte Membrane Fuel Cells. *Nat. Commun.* **2011**, *2*, 416.
(119) Yuan, S.; Shui, J.-L.; Grabstanowicz, L.; Chen, C.; Commet, S.; Reprogle, B.; Xu, T.; Yu, L.; Liu, D.-J. A Highly Active and Support-Free Oxygen Reduction Catalyst Prepared from Ultrahigh-

DOI: 10.1021/acscatal.9b02583
ACS Catal. 2019, 9, 10126−10141

Surface-Area Porous Polyporphyrin. *Angew. Chem.* **2013**, *125*, 8507−8511.
(120) Zhao, D.; Shui, J.-L.; Grabstanowicz, L. R.; Chen, C.; Commet, S. M.; Xu, T.; Lu, J.; Liu, D.-J. Highly Efficient Non-Precious Metal Electrocatalysts Prepared from One-Pot Synthesized Zeolitic Imidazolate Frameworks. *Adv. Mater.* **2014**, *26*, 1093−1097.
(121) Tang, H.; Qi, Z.; Ramani, M.; Elter, J. F. Pem Fuel Cell Cathode Carbon Corrosion Due to the Formation of Air/Fuel Boundary at the Anode. *J. Power Sources* **2006**, *158*, 1306−1312.
(122) Chen, J.; Hu, J.; Waldecker, J. R. A Comprehensive Model for Carbon Corrosion During Fuel Cell Start-Up. *J. Electrochem. Soc.* **2015**, *162*, F878−F889.
(123) Reiser, C. A.; Bregoli, L.; Patterson, T. W.; Yi, J. S.; Yang, J. D.; Perry, M. L.; Jarvi, T. D. A Reverse-Current Decay Mechanism for Fuel Cells. *Electrochem. Solid-State Lett.* **2005**, *8*, A273−A276.
(124) Ferreira-Aparicio, P.; Chaparro, A. M.; Folgado, M. A.; Conde, J. J.; Brightman, E.; Hinds, G. Degradation Study by Start-up/Shut-Down Cycling of Superhydrophobic Electrosprayed Catalyst Layers Using a Localized Reference Electrode Technique. *ACS Appl. Mater. Interfaces* **2017**, *9*, 10626−10636.
(125) Meyers, J. P.; Darling, R. M. Model of Carbon Corrosion in Pem Fuel Cells. *J. Electrochem. Soc.* **2006**, *153*, A1432−A1442.
(126) Chen, J.; Siegel, J. B.; Matsuura, T.; Stefanopoulou, A. G. Carbon Corrosion in Pem Fuel Cell Dead-Ended Anode Operations. *J. Electrochem. Soc.* **2011**, *158*, B1164−B1174.
(127) Malek, K.; Franco, A. A. Microstructure-Based Modeling of Aging Mechanisms in Catalyst Layers of Polymer Electrolyte Fuel Cells. *J. Phys. Chem. B* **2011**, *115*, 8088−8101.
(128) Dubau, L.; Castanheira, L.; Maillard, F.; Chatenet, M.; Lottin, O.; Maranzana, G.; Dillet, J.; Lamibrac, A.; Perrin, J.-C.; Moukheiber, E.; ElKaddouri, A.; De Moor, G.; Bas, C.; Flandin, L.; Caqué, N. A Review of Pem Fuel Cell Durability: Materials Degradation, Local Heterogeneities of Aging and Possible Mitigation Strategies. *Wiley Interdiscip. Rev.: Energy Environ.* **2014**, *3*, 540−560.
(129) Wang, W.; Luo, J.; Chen, S. Carbon Oxidation Reactions Could Misguide the Evaluation of Carbon Black-Based Oxygen-Evolution Electrocatalysts. *Chem. Commun.* **2017**, *53*, 11556−11559.
(130) Choi, C. H.; Baldizzone, C.; Grote, J.-P.; Schuppert, A. K.; Jaouen, F.; Mayrhofer, K. J. J. Stability of Fe-N-C Catalysts in Acidic Medium Studied by Operando Spectroscopy. *Angew. Chem., Int. Ed.* **2015**, *54*, 12753−12757.
(131) Choi, C. H.; Baldizzone, C.; Polymeros, G.; Pizzutilo, E.; Kasian, O.; Schuppert, A. K.; Ranjbar Sahraie, N.; Sougrati, M.-T.; Mayrhofer, K. J. J.; Jaouen, F. Minimizing Operando Demetallation of Fe-N-C Electrocatalysts in Acidic Medium. *ACS Catal.* **2016**, *6*, 3136−3146.
(132) Lefèvre, M.; Dodelet, J.-P. Fe-Based Catalysts for the Reduction of Oxygen in Polymer Electrolyte Membrane Fuel Cell Conditions: Determination of the Amount of Peroxide Released During Electroreduction and Its Influence on the Stability of the Catalysts. *Electrochim. Acta* **2003**, *48*, 2749−2760.
(133) Kolthoff, I. M.; Medalia, A. I. The Reaction between Ferrous Iron and Peroxides. I. Reaction with Hydrogen Peroxide in the Absence of Oxygen. *J. Am. Chem. Soc.* **1949**, *71*, 3777−3783.
(134) Barb, W. G.; Baxendale, J. H.; George, P.; Hargrave, K. R. Reactions of Ferrous and Ferric Ions with Hydrogen Peroxide. Part I.—the Ferrous Ion Reaction>. *Trans. Faraday Soc.* **1951**, *47*, 462−500.
(135) Goellner, V.; Armel, V.; Zitolo, A.; Fonda, E.; Jaouen, F. Degradation by Hydrogen Peroxide of Metal-Nitrogen-Carbon Catalysts for Oxygen Reduction. *J. Electrochem. Soc.* **2015**, *162*, H403−H414.
(136) Schulenburg, H.; Stankov, S.; Schünemann, V.; Radnik, J.; Dorbandt, I.; Fiechter, S.; Bogdanoff, P.; Tributsch, H. Catalysts for the Oxygen Reduction from Heat-Treated Iron(Iii) Tetramethoxyphenylporphyrin Chloride: Structure and Stability of Active Sites. *J. Phys. Chem. B* **2003**, *107*, 9034−9041.
(137) Wu, G.; More, K. L.; Johnston, C. M.; Zelenay, P. High-Performance Electrocatalysts for Oxygen Reduction Derived from Polyaniline, Iron, and Cobalt. *Science* **2011**, *332*, 443−447.
(138) Choi, C. H.; Lim, H.-K.; Chung, M. W.; Chon, G.; Ranjbar Sahraie, N.; Altin, A.; Sougrati, M.-T.; Stievano, L.; Oh, H. S.; Park, E. S.; Luo, F.; Strasser, P.; Dražić, G.; Mayrhofer, K. J. J.; Kim, H.; Jaouen, F. The Achilles' Heel of Iron-Based Catalysts During Oxygen Reduction in an Acidic Medium. *Energy Environ. Sci.* **2018**, *11*, 3176−3182.
(139) Martinez, U.; Komini Babu, S.; Holby, E. F.; Zelenay, P. Durability Challenges and Perspective in the Development of Pgm-Free Electrocatalysts for the Oxygen Reduction Reaction. *Curr. Opin. Electrochem* **2018**, *9*, 224−232.
(140) Zhang, G.; Chenitz, R.; Lefèvre, M.; Sun, S.; Dodelet, J.-P. Is Iron Involved in the Lack of Stability of Fe/N/C Electrocatalysts Used to Reduce Oxygen at the Cathode of PEM Fuel Cells? *Nano Energy* **2016**, *29*, 111−125.
(141) Yang, L.; Larouche, N.; Chenitz, R.; Zhang, G.; Lefèvre, M.; Dodelet, J.-P. Activity, Performance, and Durability for the Reduction of Oxygen in PEM Fuel Cells, of Fe/N/C Electrocatalysts Obtained from the Pyrolysis of Metal-Organic-Framework and Iron Porphyrin Precursors. *Electrochim. Acta* **2015**, *159*, 184−197.
(142) Chenitz, R.; Kramm, U. I.; Lefèvre, M.; Glibin, V.; Zhang, G.; Sun, S.; Dodelet, J.-P. A Specific Demetalation of Fe−N4 Catalytic Sites in the Micropores of Nc_Ar + NH3 Is at the Origin of the Initial Activity Loss of the Highly Active Fe/N/C Catalyst Used for the Reduction of Oxygen in PEM Fuel Cells. *Energy Environ. Sci.* **2018**, *11*, 365−382.

DOI: 10.1021/acscatal.9b02583
ACS Catal. 2019, 9, 10126−10141